April 2010

Comparison of Catalyst Geometries using Computational Fluid Dynamics for Methane Steam Reforming

Anne Donovan Rocheleau
Worcester Polytechnic Institute

Justin Leonard Boudreau
Worcester Polytechnic Institute

COMPARISON OF CATALYST GEOMETRIES USING COMPUTATIONAL FLUID DYNAMICS FOR METHANE STEAM REFORMING

A Major Qualifying Project Report

Submitted to the Faculty of the
WORCESTER POLYTECHNIC INSTITUTE

in partial fulfillment of the requirements for the
Degree of Bachelor of Science
In Chemical Engineering

By

Justin Boudreau _____

Anne Rocheleau _____

Date: April 2010

Approved:

_____

Dr. Anthony G. Dixon, Adviser

ABSTRACT

Steam methane reforming is a widely-used process to convert methane into a mixture of hydrogen and carbon monoxide (syngas). Due to its maturity, high efficiency, and relatively low cost, steam reforming is considered a viable option for supporting a future hydrogen economy. A conventional steam reformer consists of several hundred fixed-bed reactor tubes filled with supported nickel catalyst particles, which can vary in size and geometry.

This project proposed recommendations for better catalyst particle designs, which can help lead to more efficient steam reforming technology. Because of the high operating temperatures, it is not feasible to experimentally study what exactly is happening inside the reactor. To overcome this limitation, computational fluid dynamics was used to compare the effect of different multi-holed cylindrical catalyst geometries on heat transfer, pressure drop, and methane conversion under typical steam methane reforming conditions.

The catalyst geometries modeled were 1-hole, 3-hole, 4-hole, 4-hole with vertical grooves, and 6-hole cylinders. It was concluded that the 4-hole with grooves and 6-hole catalyst particles offered the best particle temperature distribution and reaction rate. However, the 4-hole with grooves had a significantly larger void fraction, allowing a higher mass flow rate for a set pressure drop. The 4-hole with grooves also had a lower tube wall temperature than the 6-hole case.

EXECUTIVE SUMMARY

Steam methane reforming is a widely-used process to convert methane into a mixture of hydrogen and carbon monoxide (syngas). Due to its maturity, high efficiency, and relatively low cost, steam reforming is considered a viable option for supporting a future hydrogen economy. A conventional steam reformer consists of several hundred fixed-bed reactor tubes filled with supported nickel catalyst particles, which can vary in size and geometry.

The goal of this project was to compare multi-holed cylindrical catalyst geometries and propose recommendations for better catalyst particle design, which can help lead to more efficient steam methane reforming technology. Catalyst design influences process variables such as pressure drop, conversion, and heat transfer.

A good catalyst design will have a low pressure drop to save on operating costs and have a high conversion. For steam methane reforming, heat transfer is also very important. Since the reactions that take place in steam reforming are highly endothermic, a good catalyst will allow for maximum heat transfer. Also, it's crucial that the heat transfer is uniform or else thermal stress on the reactor tube could reduce tube life significantly; a 20°C increase in the tube wall temperature can reduce the lifespan of a tube by half (Stitt, 2005). This project expanded upon the previously studied 1-hole and 4-hole geometries by extending the range of catalyst geometries: 3-hole, 6-hole, and 4-hole with vertical grooves.

COMPUTER MODELING OF THE REACTOR TUBE

Because of the high operating temperatures, it is not feasible to experimentally study what exactly is happening inside the reactor. Computational fluid dynamics (CFD) was used to overcome this limitation: a small segment of a reactor tube was modeled. Symmetry planes were applied to the sides of the tube that were cut off. The end result is a small wedge of the reactor that offers more realistic flow than traditional modeling methods. For this report, the focus was on a test particle with the surrounding particles acting as a realistic environment.

Gambit was the software used to create the geometry and mesh, which was then imported into the CFD software Fluent. For the first run reaction and energy were disabled. The purpose of this run was to let Fluent calculate a realistic inlet flow. The second run had reaction and energy enabled and used

the inlet flow profile from the first run. During the reaction run, the model was checked for convergence every couple of thousand iterations.

RESULTS

First, the results for the wall segment as a whole were studied. The pressure drop was specified as 3,376 Pa/m for all the cases, and the pressure drop stayed close to the set value for each case. As expected, as the void fraction increased, the mass flow rate increased. The average temperature of the exiting gas decreased because more mass was flowing through the tube. The average reactor tube wall temperature generally increased as the void fraction increased. However, the average temperature for the 6-hole case was more than 10 K hotter than the 3-hole case that had the same void fraction. This was due to variations in flow. In particular, the 6-hole case did not have as effective radial flow as the 3-hole case. This reduced radial heat transfer and resulted in a higher tube wall temperature.

Next, the results for the test particle itself were studied. In general, as the surface area of the particle increased, so did the amount of reaction, as evidenced by the reaction rates and heat sinks. This is expected since the reaction takes place very close to the surface of the particle. Since the dominant reactions in steam methane reforming are endothermic, a higher heat sink means more reaction is occurring.

The temperature contours of each case followed a trend with the exception of the 4-hole with grooves case. In general, as the void fraction increased, the intensity of a hotspot on the particle increased. However, the grooves in the 4-hole with grooves case created a larger gap between the particle and the tube wall. As a result, the 4-hole with grooves had a less intense hotspot despite its high void fraction.

The 4-hole with grooves also exhibited funneling caused by the grooves. When compared to the 4-hole case, it was observed that flow tended to travel along the grooves instead of being deflected away from the particle. This helped replenish reactants near the surface of the particle.

CONCLUSIONS

Both the 4-hole with grooves and 6-hole case offered a significant increase in surface area when compared to the other cases. In addition, both cases had relatively uniform temperature contours on the particle's surface. However, the 6-hole case had a lower void fraction than the 4-hole with grooves (0.62 compared to 0.72). Also, the 6-hole case had a high tube wall temperature of 1070 K compared to the 4-hole with groove's tube wall temperature of 1062 K. The lesser-holed cases had slightly lower

tube wall temperatures; however, this came at the expense of surface area and void fraction. Overall, the 4-hole with grooves offered the lowest pressure drop, high reaction, and uniform particle temperature at the expense of a slightly higher tube wall temperature when compared with the lesser-holed cases. The 4-hole with grooves case is the best compromise among the five cases examined.

TABLE OF CONTENTS

TABLE OF FIGURES

TABLE OF TABLES

INTRODUCTION

Steam methane reforming (SMR) is a widely-used process to convert hydrocarbons (mainly methane) into a mixture of hydrogen and carbon monoxide (syngas). Currently, SMR is used in the petrochemical industry for the refining of fossil fuels; it is also used in the production of ammonia. As a result of SMR's application in these industries, the process is well-known and highly efficient (around 65-75%). The cost of steam reforming is largely dependent on the price of natural gas, but currently it is one of the most economical options for hydrogen production (Hydrogen production - steam methane reforming (SMR), n.d.). Due to its maturity, high efficiency, and relatively low cost, steam reforming is considered a viable option for supporting a future hydrogen economy.

The importance of steam reforming in the refining and chemical industry today as well as the potential uses for steam reforming in the future give impetus for further study of the process. The primary reactions that take place in steam reforming are summarized in Table 1.

TABLE 1: PRIMARY STEAM REFORMING REACTIONS.

Reaction	Heat of reaction (kJ/mol)
1. $\mathbf{CH_4 + H_2O \leftrightarrow CO + 3H_2}$	-206.10
2. $\mathbf{CO + H_2O \leftrightarrow CO_2 + H_2}$	41.15
3. $\mathbf{CH_4 + 2H_2O \leftrightarrow CO_2 + 4H_2}$	-165.00

Due to the highly endothermic nature of the first and third reactions, reformers are operated at high temperatures (usually between 800 and 900 K). A conventional steam reformer consists of several hundred fixed-bed reactor tubes. These tubes are usually heated by open-flame furnaces to reach the desired temperature. Pretreated methane feed is sent down the tubular reactors where the reactions take place in the presence of a catalyst. The catalyst is usually nickel supported by alumina (Al_2O_3) pellets, which can vary in size and geometry (Bruno, Guillermo, & Gonzalez, 1988), (Kagyrmanova, Zolotarskii, Vernikovskaya, Smirnov, Kuz'min, & Chumakova, 2006). The reformed gas then exits the reactor array and is often sent for further treatment in a series of water gas shift reactions. A diagram of a typical steam reforming process can be seen in Figure 1.

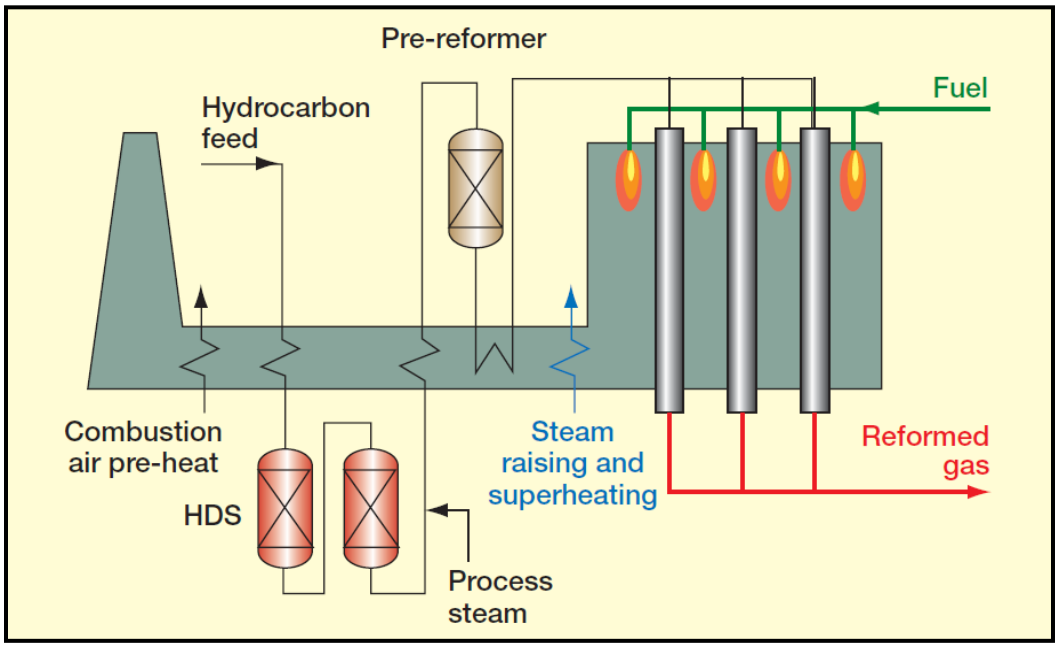

FIGURE 1: STEAM REFORMING PROCESS (BROADHURST & ABBOTT, 2002).

Although steam reforming is an efficient and cost effective method of producing hydrogen, there are several challenges associated with the process. One of the largest problems with steam reforming is the formation of hot patches and thermal banding. The reactor tubes are exposed to fired heaters and must effectively transfer heat to the catalyst particles and gas mixture inside the reactor. If heat is dissipated unevenly, temperature gradients on the tube wall can strain the tube and reduce its life span significantly. For example, a tube wall temperature increase of 20°C can reduce the tube life by half, from ten years to five years (Stitt, 2005). With the cost of re-tubing around $5-8 million, there is great incentive to maximize heat transfer. In addition to effective heat transfer, it is important to have a low pressure drop and high methane conversion. A low pressure drop allows for more methane to be processed and can reduce operating costs.

In order to overcome the challenges associated with steam reforming, it is necessary to understand the fluid mechanics, heat transfer, and reaction kinetics taking place within the reactor. Because of the high operating temperature of reformers, it is not feasible to experimentally determine exactly what is happening inside the reactors. Due to this limitation, computational fluid dynamics (CFD) is increasingly being used to model processes such as steam methane reforming in conjunction with classical reaction engineering models.

The goal of this project was to use computational fluid dynamics to compare the effect of different catalyst geometries on the following characteristics under typical steam methane reforming conditions:

- ***Heat transfer***. Good heat transfer allows for longer tube life and increased reaction.
- ***Pressure drop***. A low pressure drop allows for more methane to be processed.
- ***Methane conversion***. High methane conversion allows for more hydrogen to be produced.

The major geometric factor affecting the activity of catalyst particles is the ratio of the particle's surface area to volume. One-dimensional particle simulations imply that reaction occurs within 3-5% of the particle radius from the surface, so the reaction effects were regarded as limited to this section (Pedernera, Pina, Borio, & Bucala, 2003). Thus, high surface area will allow for more reaction to occur. Recently, multi-holed cylinders have been studied as they have a better surface area to volume ratio than cylindrical shapes of the same outside diameter and length and allow the reactant better access into the particles. Dixon et al. used CFD to compare catalyst geometries and hole sizes for non-reactive heat transfer (Dixon, Taskin, Nijemeisland, & Stitt, 2008). In 2009, further research used CFD to study reactive heat transfer for cylindrical solid, 1-hole, and 4-hole catalyst shapes (Troupel, 2009).

For the non-reactive heat transfer study, it was concluded that for a constant pressure drop multi-holed particles (3 and 4 hole) give a lower tube wall temperature at the cost of slightly worse heat transfer into the bed. The previous study on reactive heat transfer for solid, 1-hole, and 4-hole particles concluded that the 4-hole geometry allowed for better flow than the solid particles. As a result, the wall temperatures were hotter for the solid particles than the holed particles.

This project uses the grid generation software Gambit 2.4 and the CFD software Fluent 3D 6.3 to compare the previously-studied 1-hole and 4-hole geometries to an extended range of cylindrical geometries, including:

- ***3-hole***. This geometry, which includes three longitudinal, cylindrical holes arranged in a triangular configuration, was chosen for study because Kagyrmanova compared it to Raschig rings (Kagyrmanova, Zolotarskii, Smirnov, & Vernikovskaya, 2007).
- ***6-hole***. This geometry was investigated because BASF produces a six-holed cylindrical catalyst that includes one central cylindrical hole and five surrounding holes. The BASF catalyst has slightly domed ends, but for the simplification and for easier comparison with the other geometries, the 6-hole shape in this project was modeled with flat ends. This shape was designed to have a large void fraction, high surface area, and a low pressure drop (Product data, 2007).
- ***4-hole with grooves***. This geometry was analyzed because Johnson Matthey Catalysts produces a catalyst under their Katalco™ brand that is similar to the 4-hole geometry previously studied

by Troupel, but it includes four rounded grooves ("flutes") along the length of the particle (Katalco 57-series).

The cylindrical catalyst geometries studied in this paper are shown in Figure 2. With the geometry comparisons, recommendations for better catalyst particle designs were made, which can help lead to more efficient steam reforming technology.

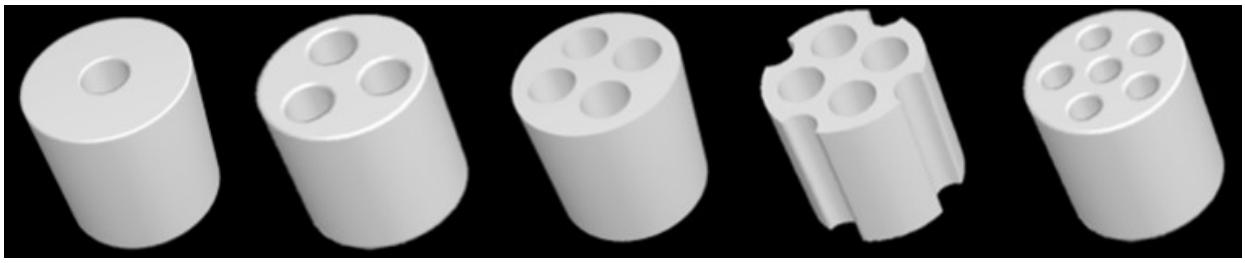

FIGURE 2: 1-HOLE, 3-HOLE, 4-HOLE, 4-HOLE WITH GROOVES, AND 6-HOLE CATALYST PARTICLE GEOMETRIES.

BACKGROUND

Good heat transfer is very important in the packed beds used in steam methane reforming. The process includes three types of heat transfer:

- ***Heat transfer on the furnace or shell side to the tube***. This includes mainly radiation as well as convection.
- ***Heat transfer through the reformer tube***. This is the tube wall conductivity, which presents the least resistance to heat transfer.
- ***Heat transfer into the catalyst bed***. This is the convection through the gas film bordering the wall into the process gas, then through the bed.

The heat transfer in a reformer tube is essentially from the tube wall to the catalyst surface, with the flowing gas as a heat transfer medium. There is also a very small amount of solid phase conduction between pellets (Stitt, 2005).

CATALYST DESIGN

The major geometric factor affecting the activity of catalyst particles is the ratio of the particle's geometric surface area to volume, SA/V. The optimization of catalyst particles for steam methane reforming includes the following (contradictory) conditions:

- ***Low pressure drop***. This requires high voidage and thus large particles.
- ***High surface area***. This leads to high activity and usually calls for small particles.
- ***Good radial mixing***. This results in better heat transfer from the wall to the center of the tube and necessitates large particles.
- ***High strength***. This avoids breakage during handling and the filling of the beds. Strength will not be addressed in this analysis of catalyst geometries, but it should be noted that although no catalyst is strong enough to resist the stresses of tube contraction during cooling, the fracture patterns are important in preventing an increase in pressure drop (Stitt, 2005).

Multi-holed cylinders (such as those shown in Figure 3) have a lower pressure drop since they have higher voidage, and they also have better SA/V, allowing the reactant better access into the particles, thus meeting these requirements better than simple cylindrical shapes of the same outside diameter and length (Sie & Krishna, 1998). The reforming industry uses particles of a length to diameter ratio in the

range of 0.8–1.2. Tube-to-particle diameter ratios (N) usually vary from 3–10 for steam methane reforming fixed bed reactors (Dixon, Nijemeisland, & Stitt, 2006). At these values of N, radial heat transfer is good, and there are only small temperature gradients across the bulk of the tube. The heat transfer from the wall to the gas has the highest resistance, and there are large temperature differences across the boundary layer (Stitt, 2005).

FIGURE 3: REFORMER TUBE PACKED WITH 4-HOLE CYLINDRICAL CATALYST PARTICLES (STITT, 2005).

MODELS FOR STEAM REFORMING

Modeling the fixed-bed tube reactors used for steam reforming has been performed using several different methods. One of the most popular methods is the two-dimensional homogeneous model. This method models the fluid and solid zones as one zone.

In one paper by Kagyrmanova et al, a two-dimensional pseudo-homogenous model was used to simulate the performance of three-holed cylinders (Kagyrmanova, Zolotarskii, Smirnov, & Vernikovskaya, 2007). The three-holed cylinders were compared to Raschig rings and conclusions were made regarding the optimal catalyst diameter and height. The results from this study indicated that the three-holed cylinders were more effective at transferring heat, had a better methane conversion, and had a lower pressure drop than Raschig rings.

CFD MODELING

Computational fluid dynamics (CFD) is a modeling technology that is used to model applications in many engineering disciplines, including aerospace, automotive, electronics, chemical, and power generation. It

is an alternative to the two-dimensional homogeneous models that have been traditionally used to simulate packed bed reactors. Increases in computer processing power have allowed for the development of increasingly complex models that can account for wall heating effects.

A randomly-packed tube (such as in Figure 3) is geometrically intricate and thus difficult to model. As the entire bed cannot be simulated, a short piece of the tube reduces the CFD calculation to a more convenient size. One of the difficulties associated with CFD is obtaining a realistic random packing while having an identical top and bottom, necessary for a periodic flow. Instead of an unrealistic uniform inlet flow, periodicity of the short piece of tube allows for a more realistic developed profile.

It has been demonstrated that the wall segment model (Figure 4), a periodic 120° segment with symmetry at the sides is a reasonable representation of the full packed bed (Nijemeisland & Dixon, 2004). The CFD approach for packed bed heat transfer was validated by comparison to experiments (Nijemeisland & Dixon, 2001). There is periodicity at the top and bottom of the model for the flow case without heat and reaction. Also, the porosity of the model has been determined, and the values agree with the porosity of an actual bed (Troupel, 2009). The tube-to-particle diameter ratio is four.

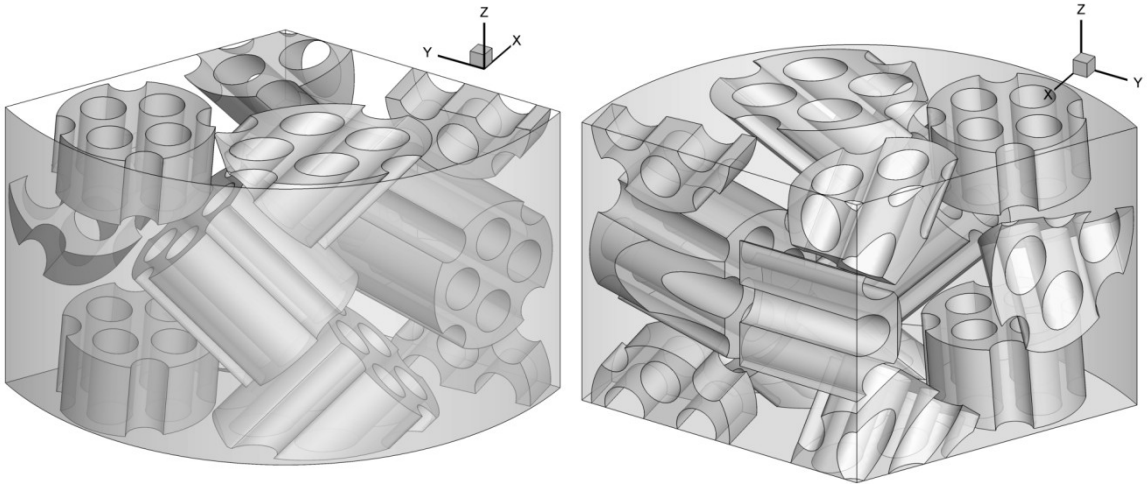

FIGURE 4: THREE-DIMENSIONAL CFD WALL-SEGMENT MODEL GEOMETRY.

MODELING TURBULENT FLOW

Steam reformers are operated with the feed gas travelling through the reactor at high velocities (on the order of 10 – 15 m/s). As a result, the flow is in the turbulent regime and cannot be fully described by the Navier-Stokes equation alone. One approach to describing turbulent flow is the use of a steady Reynolds-averaged Navier-Stokes (RANS) equation. Using this approximation, it is necessary to resolve the boundary layer as much as possible. Without a resolved boundary layer, a RANS model will not be

able to accurately predict the transition from laminar to turbulent flow. Due to this limitation, it was necessary to create a very fine mesh near the surfaces of the particles to resolve the boundary layer.

The particular RANS model used in this project was the shear-stress transport (SST) k-ω model. This model was developed by Menter to improve the accuracy of models for aeronautical applications (Menter, 1993). However, since its inception in 1993 the SST model has been applied in a variety of commercial and industrial applications beyond aeronautics.

The SST k-ω model is able to accurately model the behavior of turbulent boundary layers up to separation. Previous models, such as the k-ε model, were unable to model this behavior accurately. Another model, the standard k-ω model, is able to predict the behavior of turbulent boundary layers but does not accurately model flows with pressure-induced separation and the model is very sensitive to values of ω in the bulk flow (Menter, Kuntz, & Langtry, 2003). In order to work around this limitation, the SST k-ω model was developed. This model divides the system into zones: the near-wall region and bulk flow region. Through the use of blending functions, the SST k-ω model applies the standard k-ω model in the near-wall region while using the k-ε model for the bulk flow. Thus, the SST k-ω model combines the strength of the k-ω model near the wall and the strength of the k-ε model in the bulk flow.

REACTION KINETICS

Three major reactions (summarized in Table 1) take place during steam methane reforming. Reactions 1 and 3 consume methane and produce hydrogen along with carbon dioxide or carbon monoxide. These two reactions are highly endothermic. In addition to these two reactions, there is the water-gas shift reaction (2), which is slightly exothermic.

The overall reactions for steam methane reforming are not elementary. However, the overall reactions can be described with a reaction mechanism that consists of many elementary steps. Hou & Hughes proposed a mechanism for steam methane reforming. This mechanism operates on the following assumptions (Hou & Hughes, 2001):

1. Water adsorbs to the catalyst, yielding adsorbed oxygen and releasing gaseous hydrogen.
2. Methane attaches to the catalyst, yielding adsorbed CH_2 radicals and adsorbed hydrogen.
3. Adsorbed CH_2 and adsorbed oxygen react to yield adsorbed CHO and adsorbed hydrogen.
4. Adsorbed CHO either dissociates into adsorbed carbon monoxide and adsorbed hydrogen or it reacts with adsorbed oxygen to give adsorbed carbon dioxide and adsorbed hydrogen.

5. Adsorbed CO reacts with adsorbed oxygen to form CO_2 or the carbon monoxide can desorb into the gas phase.

The steps in the mechanism are summarized in Table 2.

TABLE 2: SMR MECHANISM.

Step	Reaction
s_1	$H_2O + s \leftrightarrow H_2 + Os$
s_2	$CH_4 + 3s \leftrightarrow CH_2s + 2Hs$
s_3	$CH_2s + Os \leftrightarrow CHOs + Hs$
s_4 (RDS)	$CHOs + s \leftrightarrow COs + Hs$
s_5 (RDS)	$COs + Os \leftrightarrow CO_2s + s$
s_6 (RDS)	$CHOs + Os \leftrightarrow CO_2s + Hs$
s_7	$COs \leftrightarrow CO + s$
s_8	$CO_2s \leftrightarrow CO_2 + s$
s_9	$2Hs \leftrightarrow H_2 + 2s$

Hou & Hughes applied the Langmuir-Hinshelwood-Hougen-Watson (LHHW) approach to develop the rate equations. By assuming that the steps four through six were rate determining steps, the following rate equations were developed (Equations 1through 4):

$$r_1 = \frac{k_1\left(\frac{P_{CH_4}P_{H_2O}^{0.5}}{P_{H_2}^{1.25}}\right)\left(1 - \frac{P_{CO}P_{H_2}^3}{K_{p1}P_{CH_4}P_{H_2O}}\right)}{DEN^2} \qquad \text{Eq. 1}$$

$$r_2 = \frac{k_2\left(\frac{P_{CO}P_{H_2O}^{0.5}}{P_{H_2}^{0.5}}\right)\left(1 - \frac{P_{CO_2}P_{H_2}}{K_{p2}P_{CO}P_{H_2O}}\right)}{DEN^2} \qquad \text{Eq. 2}$$

$$r_3 = \frac{k_3\left(\frac{P_{CH_4}P_{H_2O}}{P_{H_2}^{1.75}}\right)\left(1 - \frac{P_{CO_2}P_{H_2}^4}{K_{p3}P_{CH4}P_{H_2O}^2}\right)}{DEN^2} \qquad \text{Eq. 3}$$

$$DEN = 1 + K_{CO}P_{CO} + K_HP_H^{0.5} + K_{H_2O}\left(\frac{P_{H_2O}}{P_{H_2}}\right) \qquad \text{Eq. 4}$$

The above rate equations take the following form:

$$r_i = \frac{\alpha_i(1-\beta_i)}{DEN^2}$$

Where α represents the kinetic factor of the overall rate expression, which largely determines how quickly the reaction will proceed. Thermodynamic considerations are represented by β. If the reaction is at equilibrium, β will equal one and the overall rate of the reaction will become zero. The term in the denominator is common to all three of the reactions taking place in steam methane reforming. The denominator accounts for competitive adsorption among species.

Hou and Hughes determined the rate and equilibrium constants using the Arrhenius and van't Hoff equations (Equations 5 and 6).

$$k_i = A_i e^{-\frac{E_i}{RT}} \qquad \text{Eq. 5}$$

$$K_i = A(K_i) e^{-\frac{\Delta H_{i,a}}{RT}} \qquad \text{Eq. 6}$$

The pre-exponential factors, activation energies, and enthalpy changes are available in current literature (Hou & Hughes, 2001).

Since the CFD software, Fluent, only has gas-phase surface reactions, the reaction kinetics could not be accounted for within the program. However, Fluent allows external functions to be called from C code. The results of the user-defined functions can be stored as user-defined scalars (UDS). For this project, the reaction kinetics were defined in an external C file.

DIFFUSION

Another limitation with Fluent is that it cannot account for diffusion into the catalyst if the catalyst is modeled as a solid. Prior to the development of user-defined functions in Fluent, attempts were made to model diffusion in the catalyst particles by using porous resolved gradients (Dixon, Taskin, Stitt, & Nijemeisland, 2007), (Kolaczkowski, Chao, Awdry, & Smith, 2007). Using this method, the particles were treated as a porous fluid and the velocity of the fluid was set to zero to simulate a solid (Troupel, 2009). This approach allowed diffusion into the particles while having the particles behave as a solid because Fluent has species defined in porous regions, but not in solid regions. However, it was determined that Fluent was not forcing the no-slip condition at the "solid"-fluid boundary. Instead of setting the velocity to zero at the solid-fluid interface, Fluent used an average velocity from surrounding cells. In this project, user-defined scalars were used to mimic the behavior of species mass fractions in the solid. User-defined functions were used to specify diffusion coefficients and reaction rates.

METHODOLOGY

Gambit 2.4 was the software used to create the packed bed's geometry and then to mesh the geometry. The CFD software Fluent 3D 6.3 was then used to model the flow and reaction cases for each catalyst shape.

GEOMETRY AND MESHING

Gambit was the software used to create the packed bed's geometry for each catalyst shape and then to mesh the geometry. The cylinder and particle geometry was based on previous packed-bed models (Nijemeisland, 2003), (Taskin, 2007); it was a 120°-wedge with two planes of symmetry and had periodicity on the top and bottom planes. The wedge contained twelve particles and had a tube-to-particle diameter ratio of four. Each particle was created at the origin and then translated and rotated to its final position (see Appendix A: Particle Placement Table). One full test particle was located at the center of the middle row (labeled "2" in Figure 5).

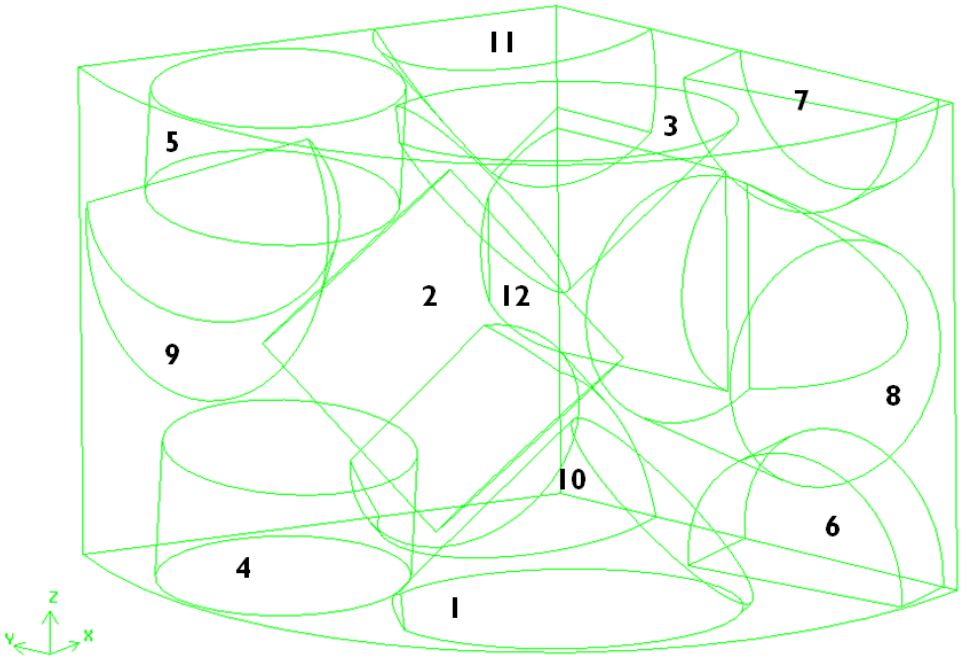

FIGURE 5: THREE-DIMENSIONAL WEDGE GEOMETRY WITH PARTICLE NUMBERING FOR REFERENCE.

The packed-bed tube section had a 2-inch radius and a height of 2 inches, and the particles had radii of 0.5 inches and lengths of 1 inch. In all but the 6-hole case, the particle holes had a radius of 0.1434 inches; for the 6-hole case, the holes had a radius of 0.1 inches in order for all the holes to fit in the

particle. The 4-hole with grooves case had grooves that were 0.12 inches in radius. Examples of the 3-hole, 4-hole with grooves, and 6-hole catalyst particles are shown in Figure 2.
The journal files to create the geometry and mesh were modified from existing journal files (Dixon, 2009) used to create the 1-hole and 4-hole geometries; an example is shown in Appendix B: Sample Gambit Journal File.

After the geometry of the particles was modified, the fluid and particle faces were connected and labeled. Then, the corresponding vertices on the top and bottom planes of the wedge were linked for periodicity using reverse orientation. The zones were defined: the top and bottom planes as well as the cylinder wall were designated as walls, the particle volumes were designated as solids, and the remaining volume was designated as fluid.

Continuous, uniform boundary layers were then added to the cylinder wall and particles (shown in Figure 6). There were three parameters used when setting the boundary layers: height of the first layer (a); growth factor (b/a), the ratio of the height of the second layer over the height of the first layer; and the number of layers. The values of these parameters for each of the cases can be found in Appendix C: Boundary Layers. These three parameters determine the total height of the boundary layer, called depth.

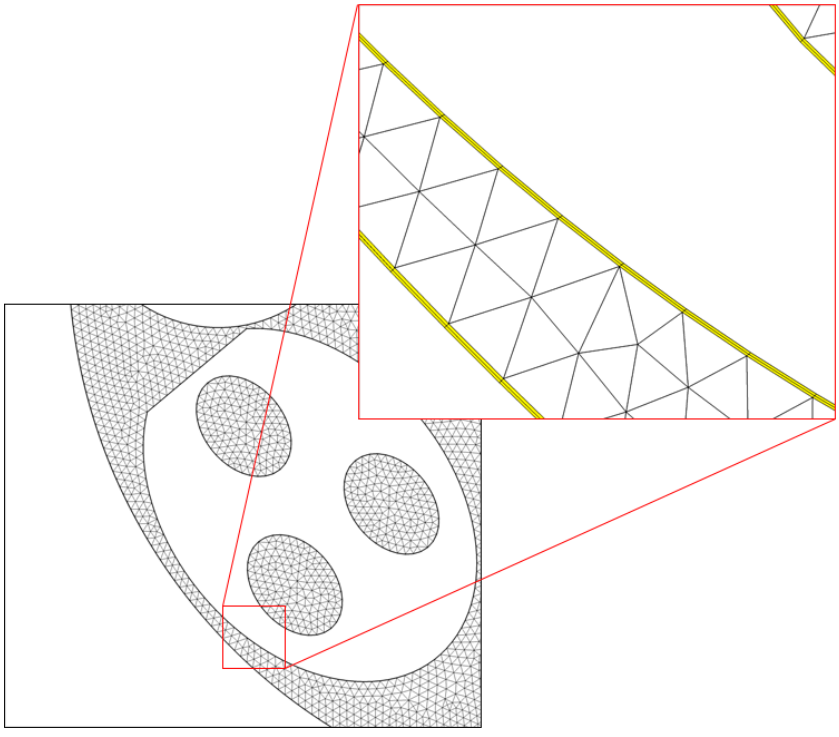

FIGURE 6: CLOSE-UP OF WALL AND PARTICLE BOUNDARY LAYERS.

The values were based off of values used previously in the 4-hole case (Troupel, 2009); they vary from particle to particle because as many as possible were added. The inner boundary layers are inside the solid particles and the outer boundary layers extend from the particle surfaces into the fluid. Not all of the particles were able to have boundary layers attached as meshing problems resulted, but as the particles were far from the particle of interest, this was acceptable.

After pre-meshing difficult edges and faces, meshing of the geometry was completed using a uniform tetrahedral mesh of 0.03 inches (Figure 7). Both the solid particles and the fluid were meshed because transport occurred in both zones. Finally, the mesh file was exported for use in the computational fluid dynamics software.

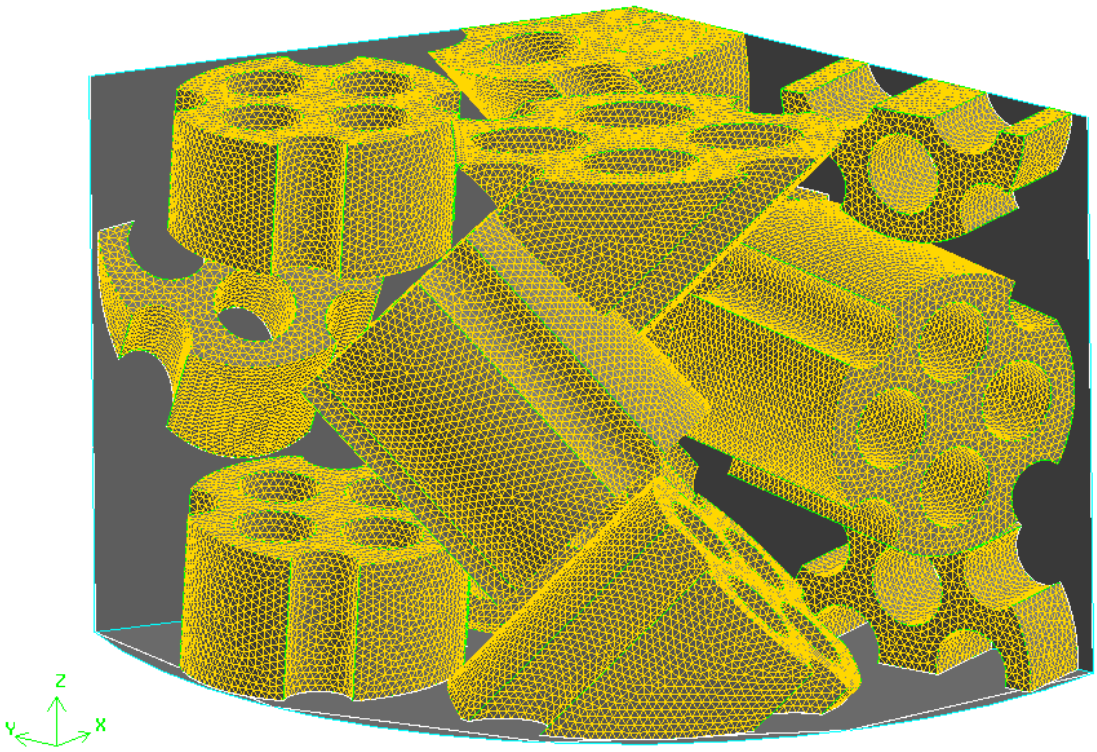

FIGURE 7: EXAMPLE OF GAMBIT PARTICLE MESH FOR 4-HOLE WITH GROOVES CASE.

COMPUTATIONAL FLUID DYNAMICS MODELING

Fluent was the computational fluid dynamics software that used the Gambit meshes. Since the Gambit files were specified in inches, Fluent's grid scale option was used to give final results in meters. The user-defined function (UDF) found in the C code (Dixon, 2009) was read to specify the source terms in the

balance equations. The parameters used in Fluent are explained below; any parameters not specifically mentioned can be assumed to be Fluent's default settings.

SIMULATION MODEL DEVELOPMENT

Fluent 3D's pressure-based solver was used for the calculations. The parameters used under these settings were absolute velocity formulation, the Green-Gauss node based gradient option, implicit formulation, steady time, and superficial velocity porous formulation. The model also used the energy equation and the SST k-ω model with the transitional flow option enabled.

The specified conditions at the reactor inlet were taken from a Johnson Matthey detailed reformer model of a methanol plant steam reformer at typical operating conditions (Nijemeisland, Dixon, & Stitt, 2004). The reactor inlet conditions and the applied boundary conditions are shown in Table 3.

TABLE 3: REACTOR CONDITIONS AND FLUID AND SOLID PROPERTIES.

REACTOR CONDITIONS

Inlet Temp, T_{in} (K)	Heat Flux, q_{wall} (kW/m^2)	Operating Press, P (kPa)	Inlet Velocity, V_{in} (m/s)
824.15	113.3	2,159	3.2

FLUID PROPERTIES

Heat Capacity, Cp (J/kg K)	Thermal Conductivity, k_f (W/m K)	Viscosity, M (Pa s)
2395.38	0.0876	$3 \cdot 10^5$

SOLID PROPERTIES

Density, ρ (kg/m^3)	Heat Capacity, Cp (J/kg K)	Thermal Conductivity, k_f (W/m K)
1947	1000	1

The fluid through the packed bed was a mixture of methane, hydrogen, carbon monoxide, carbon dioxide, and water vapor. The mixture was assumed an ideal gas with properties listed in Table 3. The mass diffusivities were dilute-approx and their values are listed in Table 4. The solid material used for the catalyst particles was alumina (Al_2O_3); the inputted property values are shown in Table 3. The UDS diffusivities for both the fluid and solid (in kg/m-s) were defined by UDFs.

Gravity was ignored, and the cylinder wall was modeled with as a stationary wall with a no-slip shear condition. The operating pressure and heat flux are specified in Table 3. The bottom was specified as a velocity inlet and fluid species mass fractions are listed in Table 4. The water mass fraction was not specified and was calculated through a mass balance. The top was specified as a pressure outlet with no gauge pressure, and backflow total temperature and species mass fractions as in the velocity inlet.

TABLE 4: SPECIES MASS DIFFUSIVITIES AND MASS FRACTIONS.

User Scalar Number	Species	Mass Diffusivity (m^2/s)	Mass Fraction
0	Methane	$1.23 \cdot 10^{-5}$	0.1966
1	Hydrogen	$2.25 \cdot 10^{-5}$	0.0005
2	Carbon monoxide	$7.2 \cdot 10^{-6}$	0.0007
3	Carbon dioxide	$4.9 \cdot 10^{-6}$	0.1753

The particles were modeled as stationary walls with a no-slip shear condition with zero species diffusive flux. UDS boundary conditions were set for specified value for each component, and the UDS boundary values were defined by the UDF. The values were computed to give continuity of flux across the interface. The faces of the particles that touch the top, bottom, or symmetry planes had no heat flux or heat generation rates specified.

SOLVING AND ANALYSIS

Two runs were needed to obtain the final case for each particle geometry. The first one was flow-only (isothermal, non-reacting), where the inlet and outlet were periodically linked together, and the pressure drop was set to 3376 Pa/m. The top profile was saved in order to have a non-uniform velocity profile for the inlet, which is more realistic than a constant inlet velocity value. In the second case, both flow and reaction (including energy) were taken into consideration. This case was non-periodic, and the velocity profile from the flow case was used for the inlet flow.

For the first run, Fluent was initialized with the settings listed in Table 5, along with the fluid species mass fractions given in Table 4. About 14,000 iterations were run and the top profile with x, y, and z-velocities as well as the turbulent kinetic energy (k) and the specific dissipation rate (omega) was saved.

TABLE 5: INITIALIZATION CONDITIONS.

Temp. (K)	Velocity (m/s)	Turbulent Kinetic Energy (m^2/s^2)	Specific Dissipation Rate (1/s)
824.15	3.2	0.256	$4.3 \cdot 10^4$

Next, the second run was set up with the original mesh. The flow run top profile was read and after initialization, approximately 20,000 – 27,400 iterations were run until convergence was achieved. In order to ease convergence, a "bootstrap" procedure was used to increase the solid density (and thus increase the reaction) up to the actual value. About twenty iterations were run using 1% of the density value. Next, the density was increased to 10% of its actual value and another twenty iterations were run. Finally, the density was increased to its actual value.

The bootstrap procedure was also used to refine the mass fractions for the fluid backflow. First, about five iterations were run using the mass fraction values from Table 4. Then, the updated mass fractions were inserted for the UDSs and two or three more iterations were run. The updated mass fractions were again inserted into the simulation until the difference between each check was less than 10^{-3}. Finally, the case was run at the full density value with refined backflow mass fractions until convergence, approximately five to eight days later, depending on the available computer resources.

To check for convergence, the reaction rates for each of the three reactions and the four species were checked periodically, approximately every 3000 iterations. The simulations were considered converged when the percent difference between checks had an order of magnitude lower than 0.1%.

RESULTS

The goal of the project was to compare the following characteristics for the previously studied 1-hole and 4-hole geometries with an extended range of catalyst geometries (3-hole, 6-hole, 4-hole with grooves):

- The temperature gradient of the test particle.
- The total heat sink and reaction rates of the test particle.
- The overall mass flow rate for a set pressure drop.

FLUENT POST-PROCESSING

The simulations were carried out on a system of parallel computers running 64-bit Red Hat Enterprise (Release 4). The server had two dual-core AMD Opteron 2220 processors running at 2.8 GHz with a 1 MB cache and 12 GB of RAM. Each model had about 2 million cells and was run for about 6000 iterations for the flow-only run. For the reaction runs, convergence occurred for the 3-hole, 4-hole with grooves, and 6-hole cases after about 24,700 iterations (approximately 185 hrs); 24,700 iterations (165 hrs); and 20,000 iterations (about 135 hrs), respectively. Convergence was checked by graphing the residuals and examining two user-created monitors, mass fraction and reaction rate, in Excel.

OVERALL RESULTS

Table 6 is a summary of the quantitative results for the reactor wedge for each of the five catalyst geometries. With additional holes, the void fraction increases; the exception is the 6-hole case because the hole diameters were smaller in order to fit on the particle. The void fractions for the 3-hole and 6-hole geometries are equal, which provides a common base for comparison. The pressure drop was specified as 3,376 Pa/m and should ideally stay the same for all the cases. However, due to flow variations from case to case, the actual pressure drops varied within 5% of the set pressure drop.

Some trends can be observed from Table 6. Mass flow rate increases as void fraction increases; this is expected since the pressure drop is held constant. There is a slight trend between void fraction and average wall temperature; in general, as the void fraction increases, the average tube wall temperature increases. However, there is a notable exception: both the 3-hole and 6-hole cases have the same void fraction but the average tube wall temperature for the 6-hole case is more than 10 K higher than the 3-

hole. Finally, the average exiting gas temperature decreases as the void fraction increases. This is due to the fact that more mass is flowing through the system at higher void fractions.

TABLE 6: SUMMARY OF RESULTS FOR REACTOR WEDGE.

Catalyst Geometry	Void Fraction	Pressure Drop (Pa/m)	Mass Flow Rate (kg/s)	Average Tube Wall Temp. (K)	Average Temp. of Exiting Gas (K)
1-hole	0.54	3372	0.02875	1055.6	829.7
3-hole	0.62	3277	0.03279	1058.4	829.5
4-hole	0.66	3176	0.03407	1057.7	828.2
4-hole with grooves	0.72	3285	0.03812	1062.0	827.0
6-hole	0.62	3334	0.03218	1070.0	828.4

Table 7 is a summary of the results of each case for the test particle specifically. With greater catalyst particle surface area, total heat sink and particle surface heat flux increase. The surface methane flow in the table should be equal to the sum of the rates of reactions 1 and 3, and the results agree with this with about 1% error. As surface area increases, reaction rate also increases. This is reasonable because reaction only takes place in the outer 3-5% of the particle's surface, and adding holes or grooves increases the surface area. Finally, there is the weighted average temperature of the test particle's surface. Since there was no distinguishable trend, it was necessary to examine the temperature contours of each particle.

TABLE 7: SUMMARY OF RESULTS FOR TEST PARTICLE.

Catalyst Geometry	Surface Area (m^2)	Weighted-Average Temp (K)	Total Heat Sink (W)	Particle Surface Heat Flux (W)	Methane Flow (kmol/s)	Reaction Rate 1 (kmol/s)	Reaction Rate 2 (kmol/s)	Reaction Rate 3 (kmol/s)
1-hole	0.00354	802.3	43.67	43.72	-2.61E-7	1.43E-8	-4.06E-9	2.46E-7
3-hole	0.00453	803.5	56.71	56.72	-3.38E-7	1.91E-8	-5.21E-9	3.19E-7
4-hole	0.00503	803.5	64.04	64.09	-3.82E-7	2.19E-8	-6.08E-9	3.59E-7
4-hole w/ grooves	0.00520	803.1	64.85	64.77	-3.88E-7	2.18E-8	-6.06E-9	3.64E-7
6-hole	0.00523	803.4	65.73	65.98	-3.92E-7	2.22E-8	-6.11E-09	3.63E-07

TEMPERATURE COMPARISON

The high temperature seems to be localized near the bottom of the test particle (see Figure 8). In general, as the void fraction increases the intensity of the hot spot increases. Despite the fact that the 6-hole case has the most holes, its void fraction is similar to the 3-hole case. This explains why the two particles have similar temperature contours. The 4-hole with grooves case has the highest void fraction but does not have the most intense hotspot. This contradicts the general trend seen in the other cases.

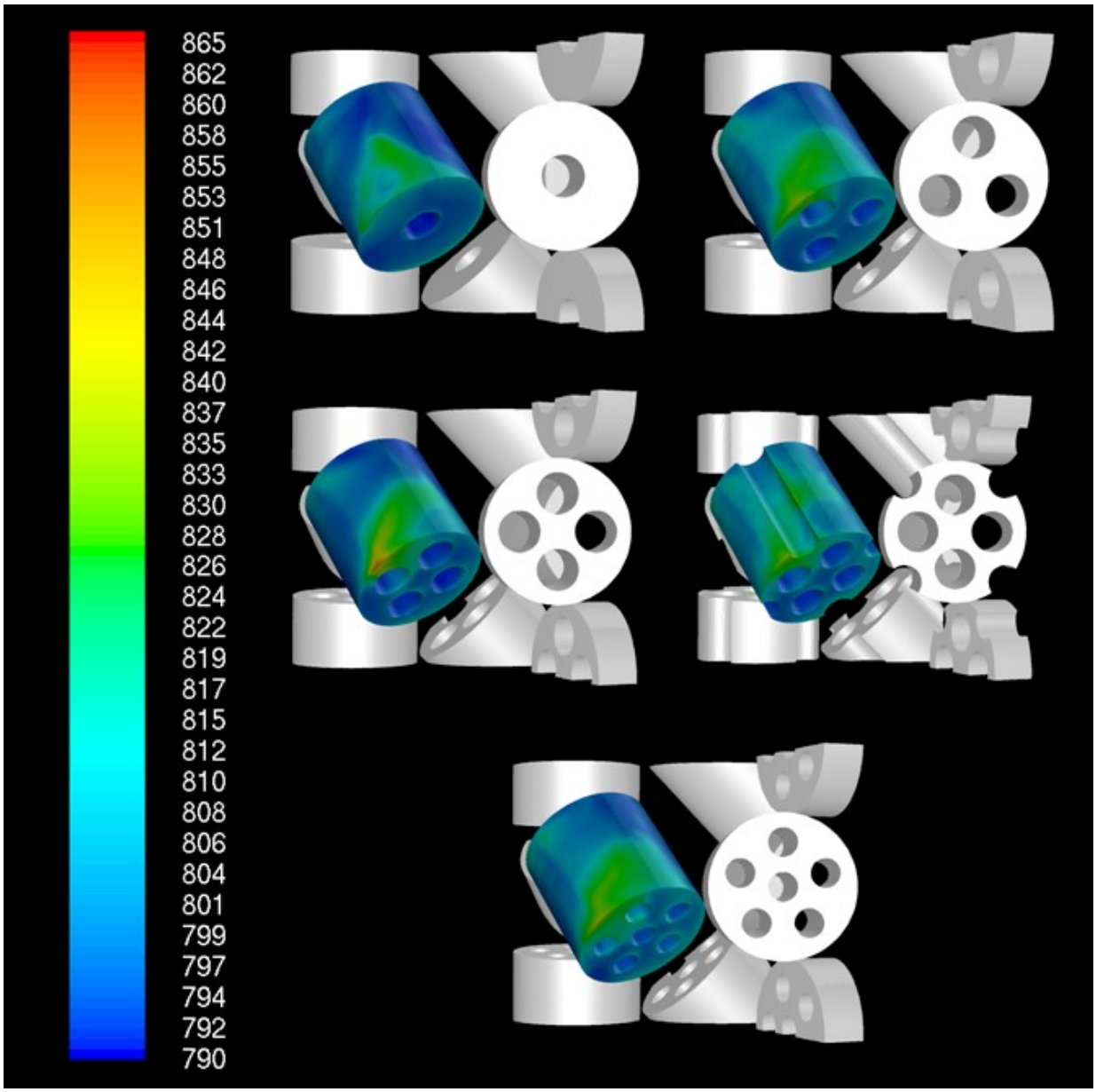

FIGURE 8: TEST PARTICLE TEMPERATURE (K) GRADIENT COMPARISONS (PARTICLES 3 AND 7 REMOVED).

To get a better understanding of why the 4-hole with grooves case has a more uniform temperature contour despite its high void fraction, a cross-sectional plane of the wedge was taken at the hotspot location. The location of the cross-sectional plane can be seen in Figure 9.

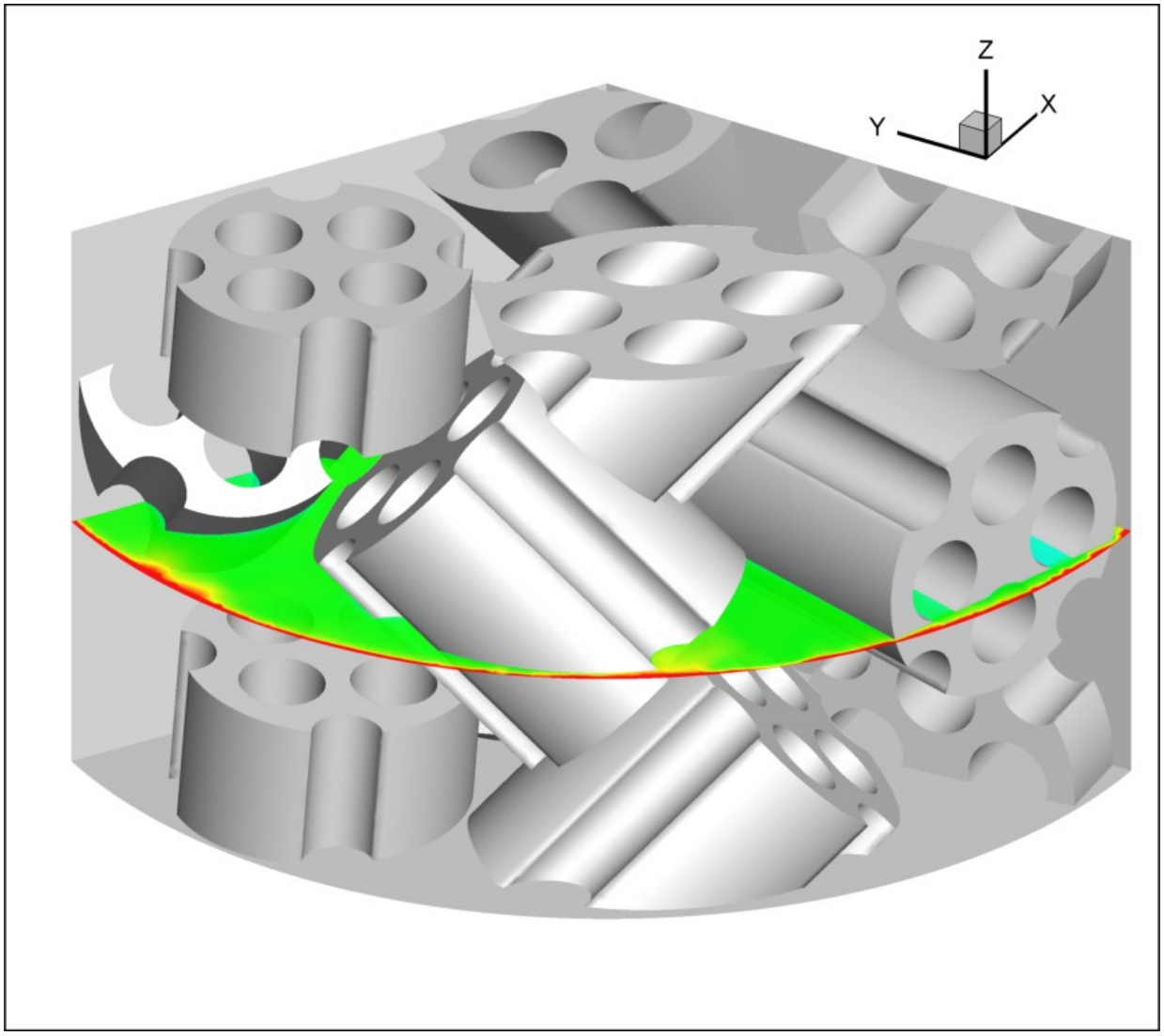

FIGURE 9: CROSS-SECTIONAL PLANE AT HOT SPOT FOR THE 4-HOLE WITH GROOVES.

Initially, it was suspected that the grooves allowed for better flow near the hotspot. This would result in increased convective heat transfer and a lower temperature. However, upon examination of the velocity contours through the cross-sectional plane, it was determined that flow variations from the two cases did not explain the reduced hotspot in the 4-hole with grooves case. The velocity contours at the cross-sectional plane can be seen in Figure 10. Close examination of the velocity contours reveals that there is stagnant flow near the hotspot (circled in red) for the 4-hole with grooves. This stagnant flow would result in less effective heat transfer; the exact opposite of what was expected.

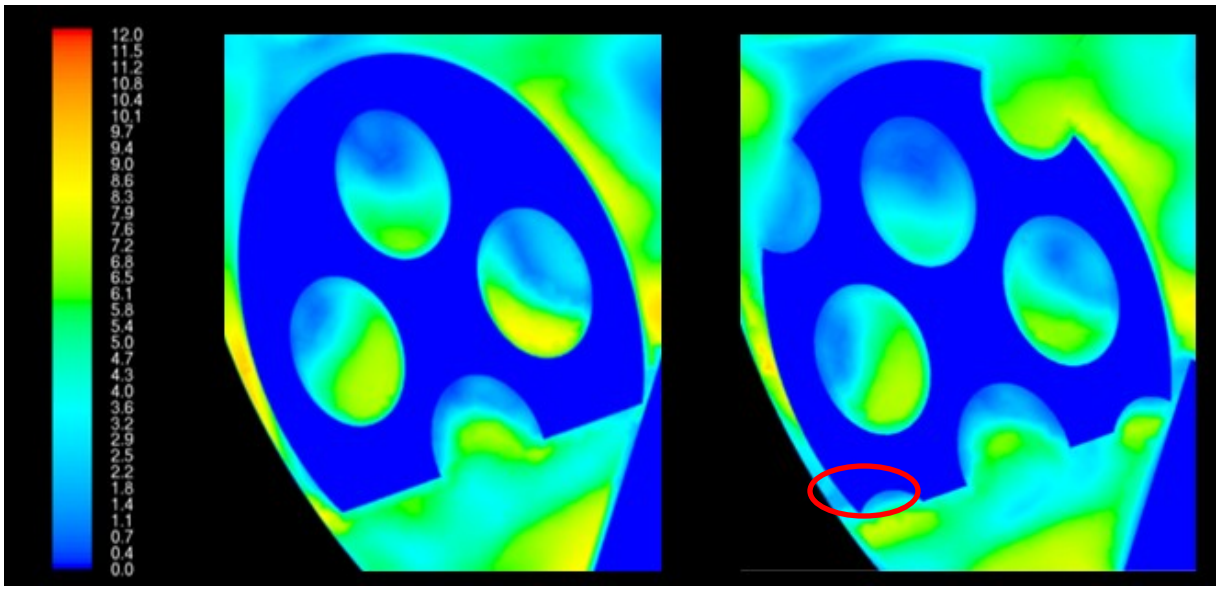

FIGURE 10: VELOCITY CONTOURS (M/S) PLANE FOR 4-HOLE CASES WITH AND WITHOUT GROOVES.

Since the velocity contours near the hotspot did not explain the reduced intensity of the spot in the 4-hole with grooves case, it was necessary to take a closer look at the temperature profile at the cross-sectional plane (Figure 11). It can be seen that the groove creates a larger gap between the particle and the tube wall. The increased distance between the particle's surface and tube wall explains why the hotspot was less intense in the 4-hole with grooves case than the 4-hole case.

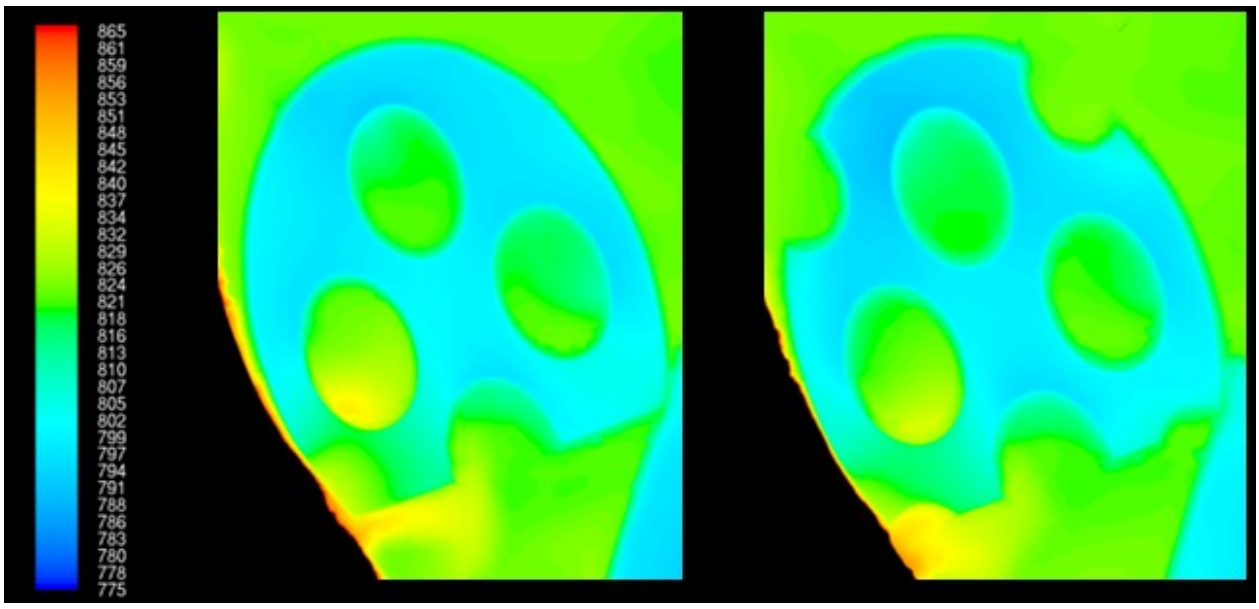

FIGURE 11: TEMPERATURE (K) CONTOURS PLANE FOR 4-HOLE CASES WITH AND WITHOUT GROOVES.

Figure 12 shows the location of another cross-sectional plane in the reactor wedge (slightly above the cross-sectional plane used to compare the 4-hole and 4-hole with grooves cases). Figure 13 depicts the cross-sectional area temperature contours for each of the five cases.

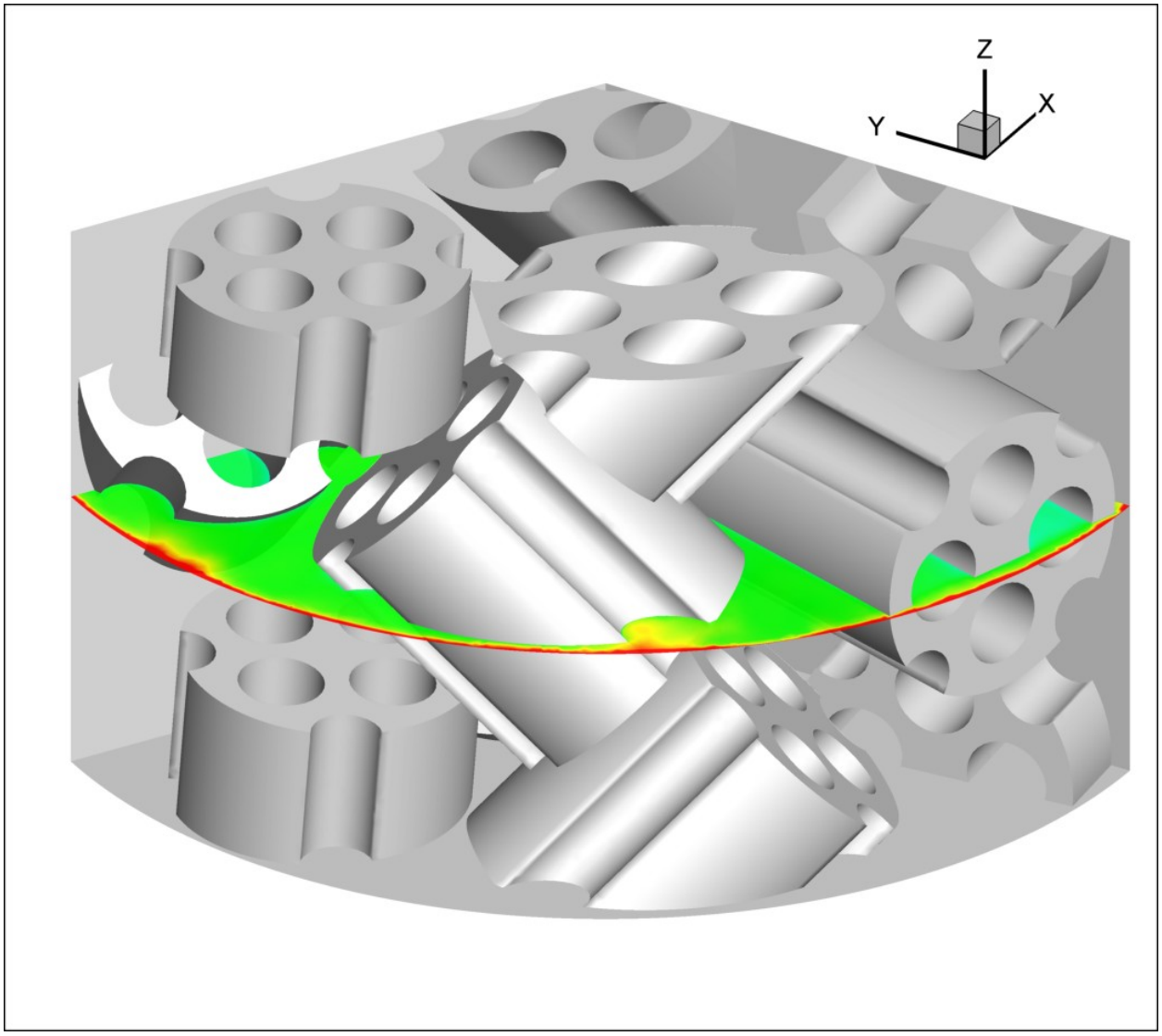

FIGURE 12: SECOND CROSS-SECTIONAL PLANE FOR THE 4-HOLE WITH GROOVES.

The cross-sectional plane helps explain why the intensity of the hotspot increases as the void fraction increases. The holes within the particle allow for hot gas to pass through the holes near the hotspot (distinguished by red arrows). The hot gas flowing through these holes heats the particle even further, resulting in more intense hotspots. This is especially noticeable when comparing the 1-hole to the multi-holed cases. In the 1-hole case, there are no holes near the hotspot while in the other cases there are

one or more holes that contain hot gas near the hotspot. Again, it can also be seen how the grooves create distance between the particle and tube wall, resulting in a less intense hotspot.

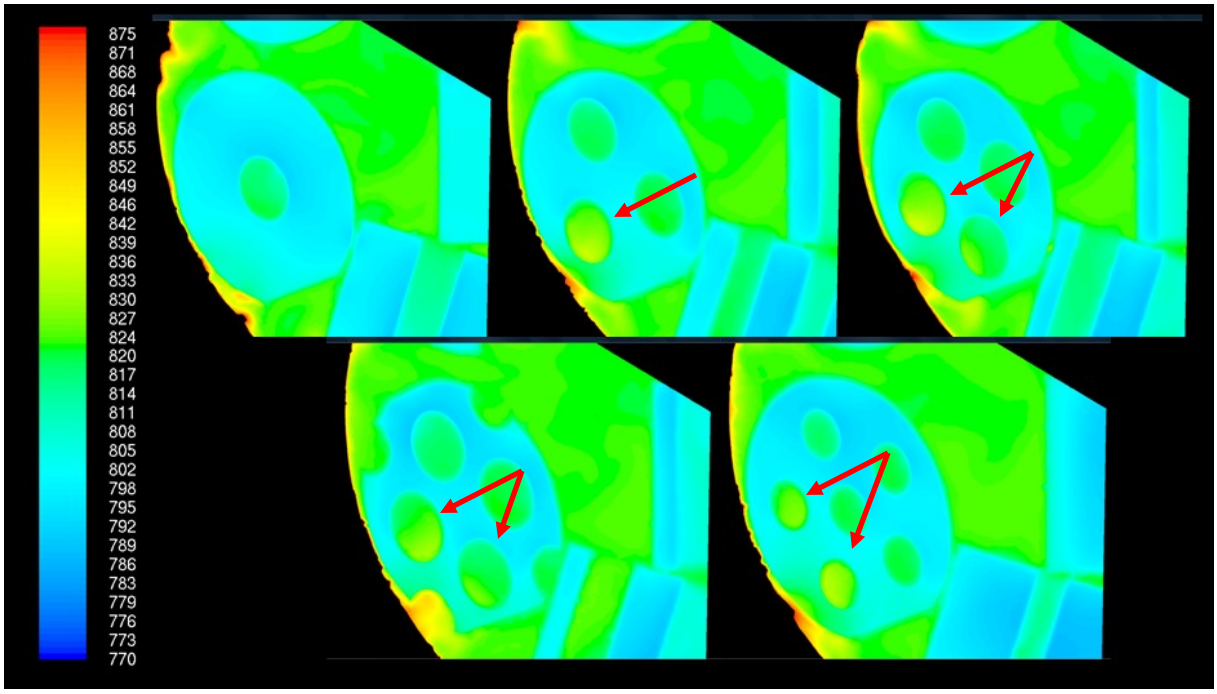

FIGURE 13: CROSS-SECTIONAL REACTOR WEDGE COMPARISONS OF TEMPERATURE (K) GRADIENT.

The radial temperature profiles within the test particle (see location in Figure 14) were compared for each of the five cases (Figure 15, Figure 16, Figure 17, Figure 18, and Figure 19). All five graphs show a slight decrease (no more than 5 K) in the particle's temperature near position 0 where the particle is closest to the inside of the reactor.

The 1-hole and 3-hole cases (Figure 15 and Figure 16, respectively) both have one bump accounting for a hole in the geometry. The 4-hole, 4-hole with grooves, and 6-hole cases (Figure 17, Figure 18, and Figure 19, respectively) all have two bumps representing two holes in the geometry. The temperature is higher in these regions (about 815–827 K) than within the catalyst because the holes contain the gaseous fluid, which enters the wedge at 824.15 K.

After the holes, the temperature increases as a result of convection as the points within the particle get closer to the heated reactor wall. All of the cases have steep temperature increases starting around 0.026 inches from the inside of the reactor where the tube wall boundary layer begins.

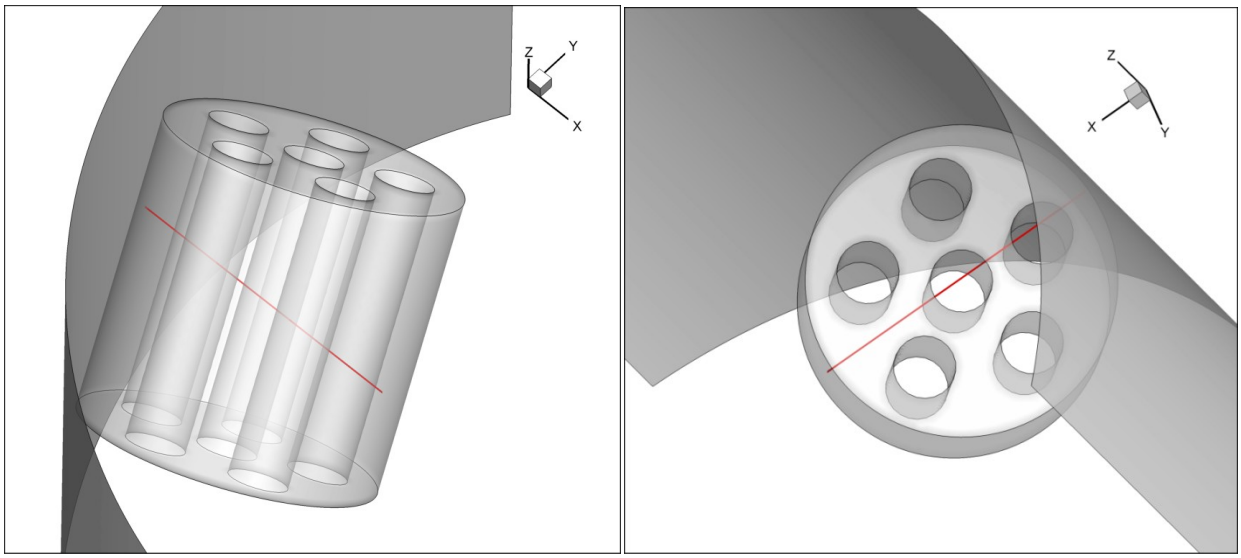

FIGURE 14: RADIAL TEMPERATURE PROFILE LINE (GOING INTO PARTICLE) FOR 6-HOLE CASE.

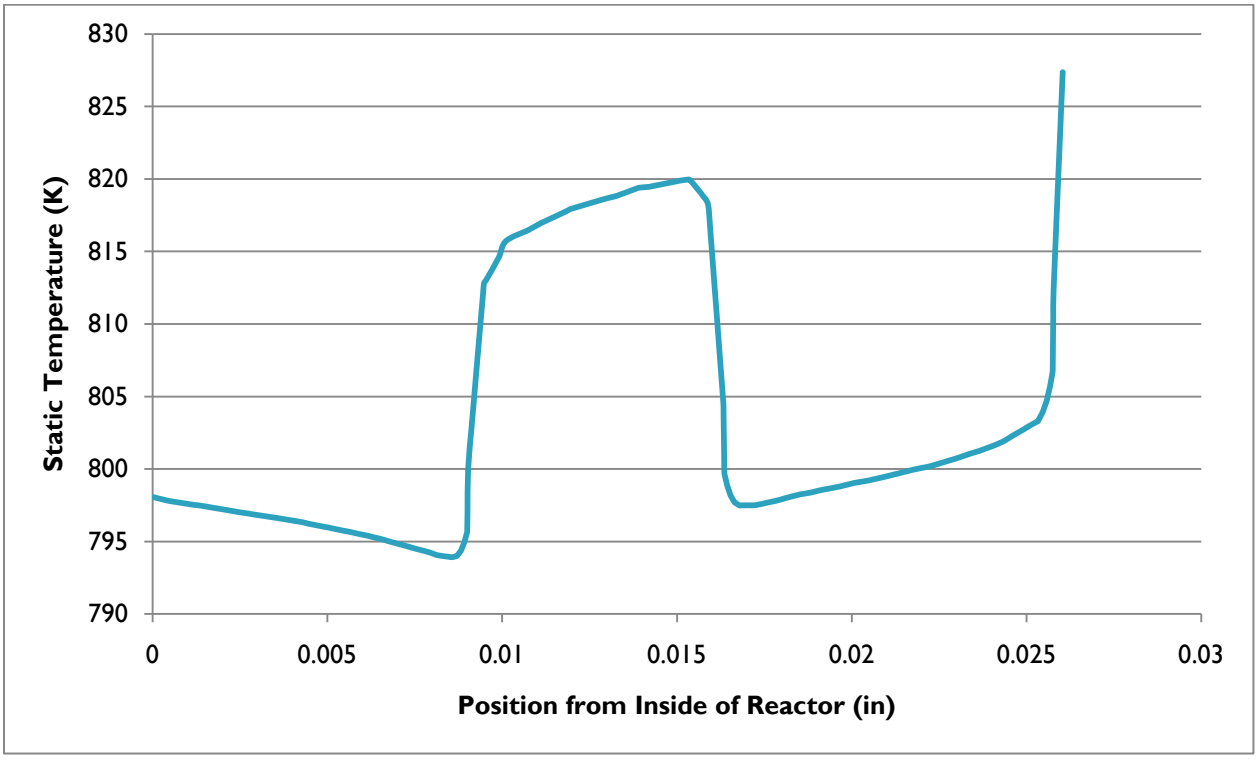

FIGURE 15: RADIAL TEMPERATURE PROFILE WITHIN TEST PARTICLE FOR 1-HOLE CASE.

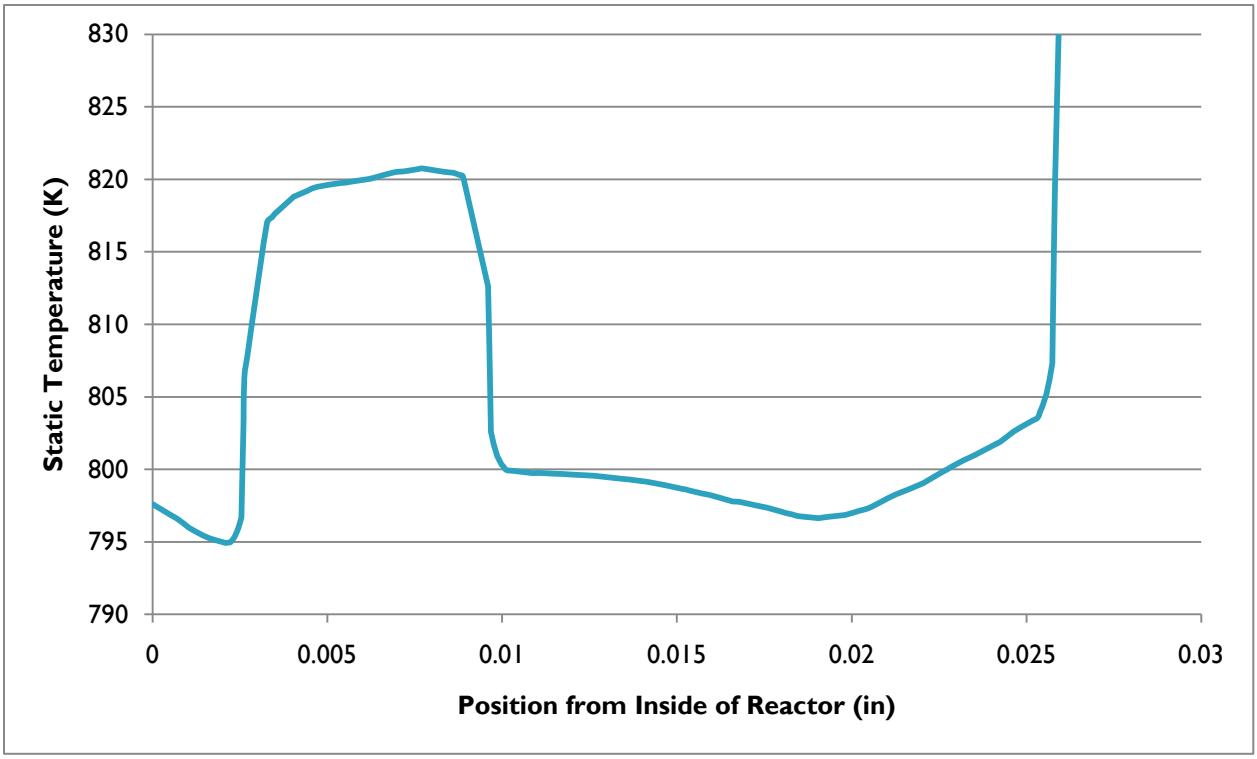

FIGURE 16: RADIAL TEMPERATURE PROFILE WITHIN TEST PARTICLE FOR 3-HOLE CASE.

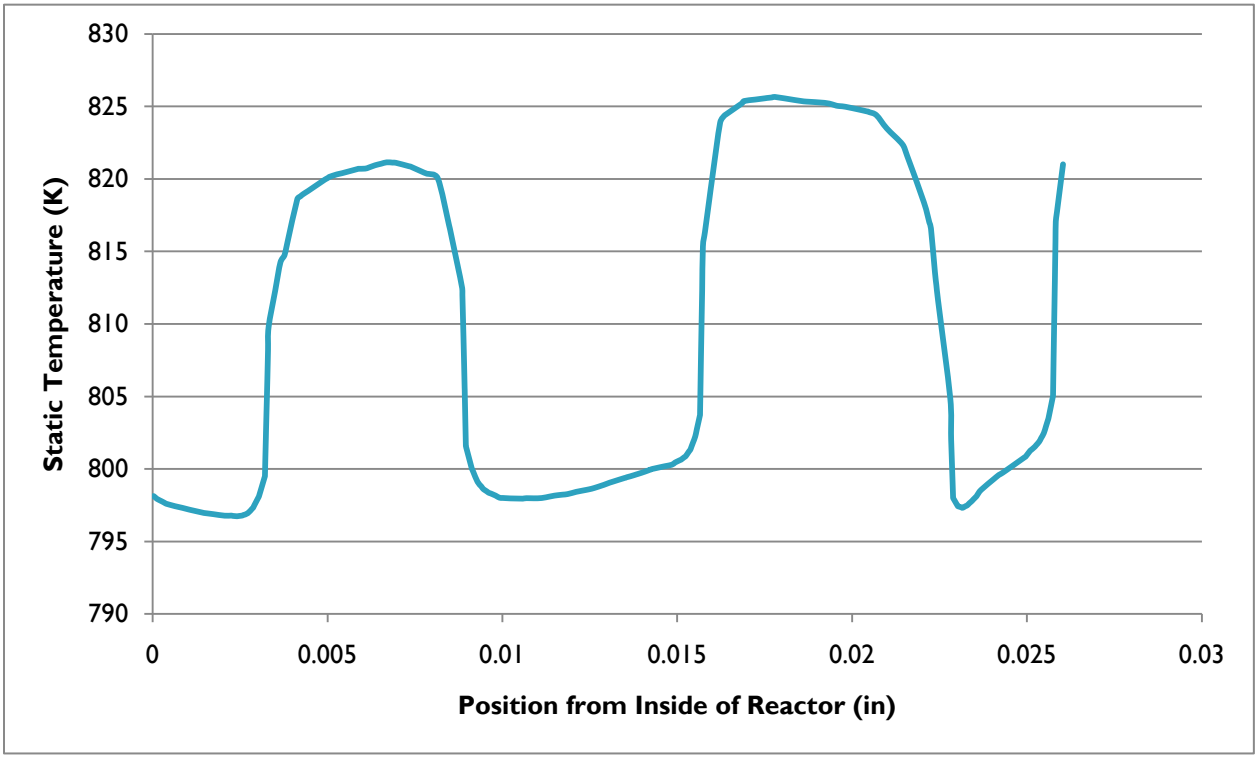

FIGURE 17: RADIAL TEMPERATURE PROFILE WITHIN TEST PARTICLE FOR 4-HOLE CASE.

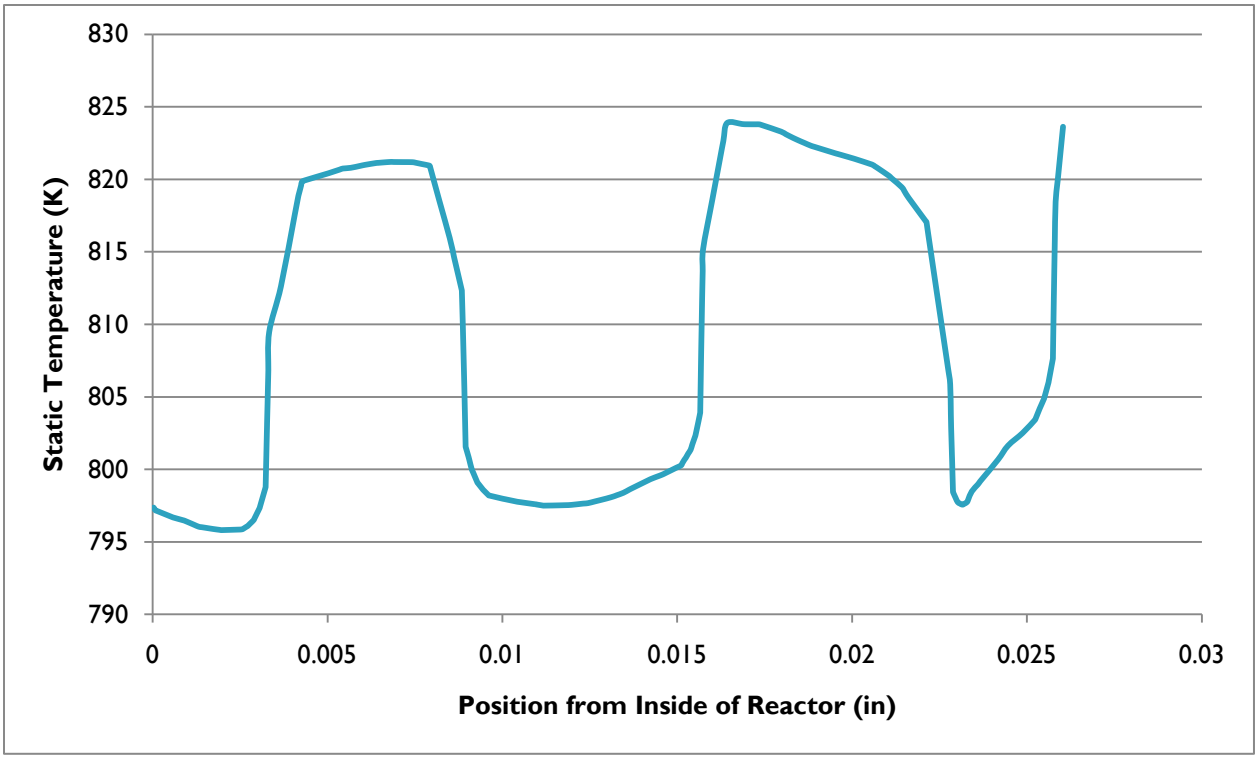

FIGURE 18: RADIAL TEMPERATURE PROFILE WITHIN TEST PARTICLE FOR 4-HOLE WITH GROOVES CASE.

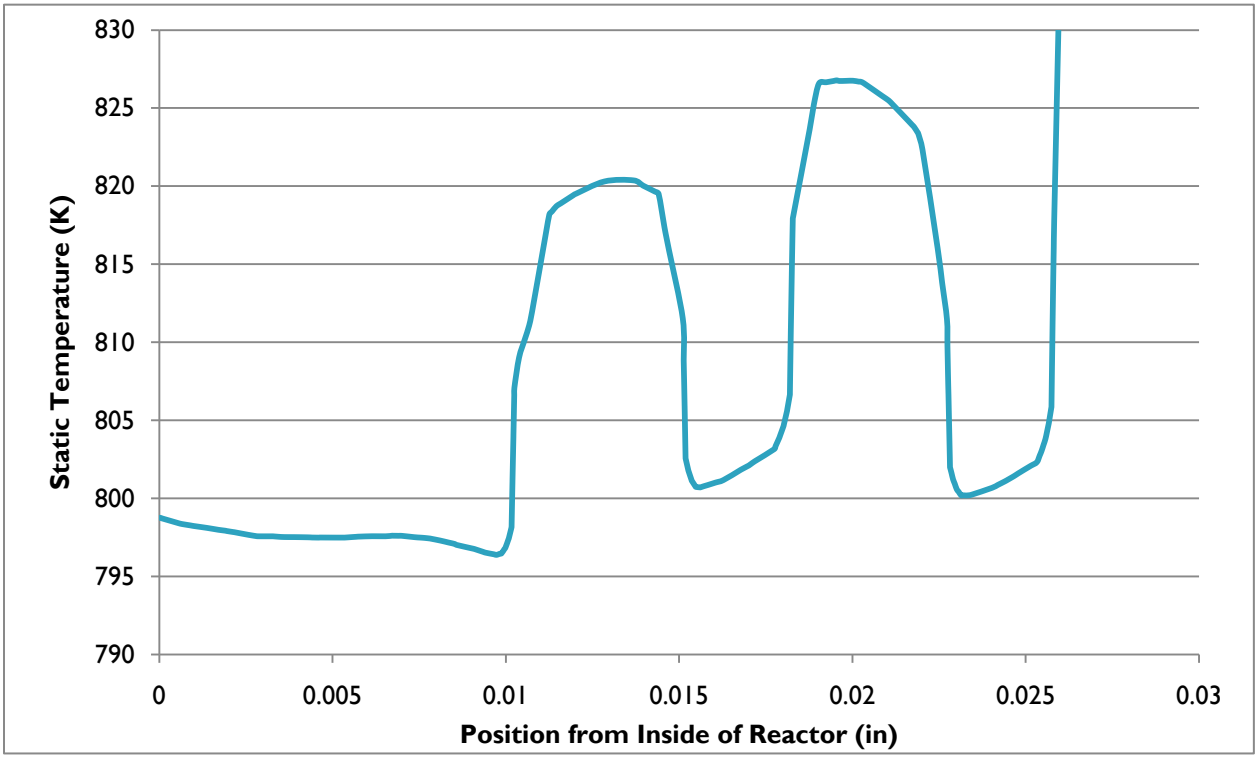

FIGURE 19: RADIAL TEMPERATURE PROFILE WITHIN TEST PARTICLE FOR 6-HOLE CASE.

FLOW FIELD COMPARISON

Figure 20 compares the velocity pathlines through the reactor wedge for each case. It can be seen that flow is faster around the surface of the test particle in the 1-hole case than the multi-holed case. Flow elsewhere in the 1-hole case also appear to be more intense than the multi-holed cases. It's also worth noting that some of the grooves appear to funnel flow along the length of the particle.

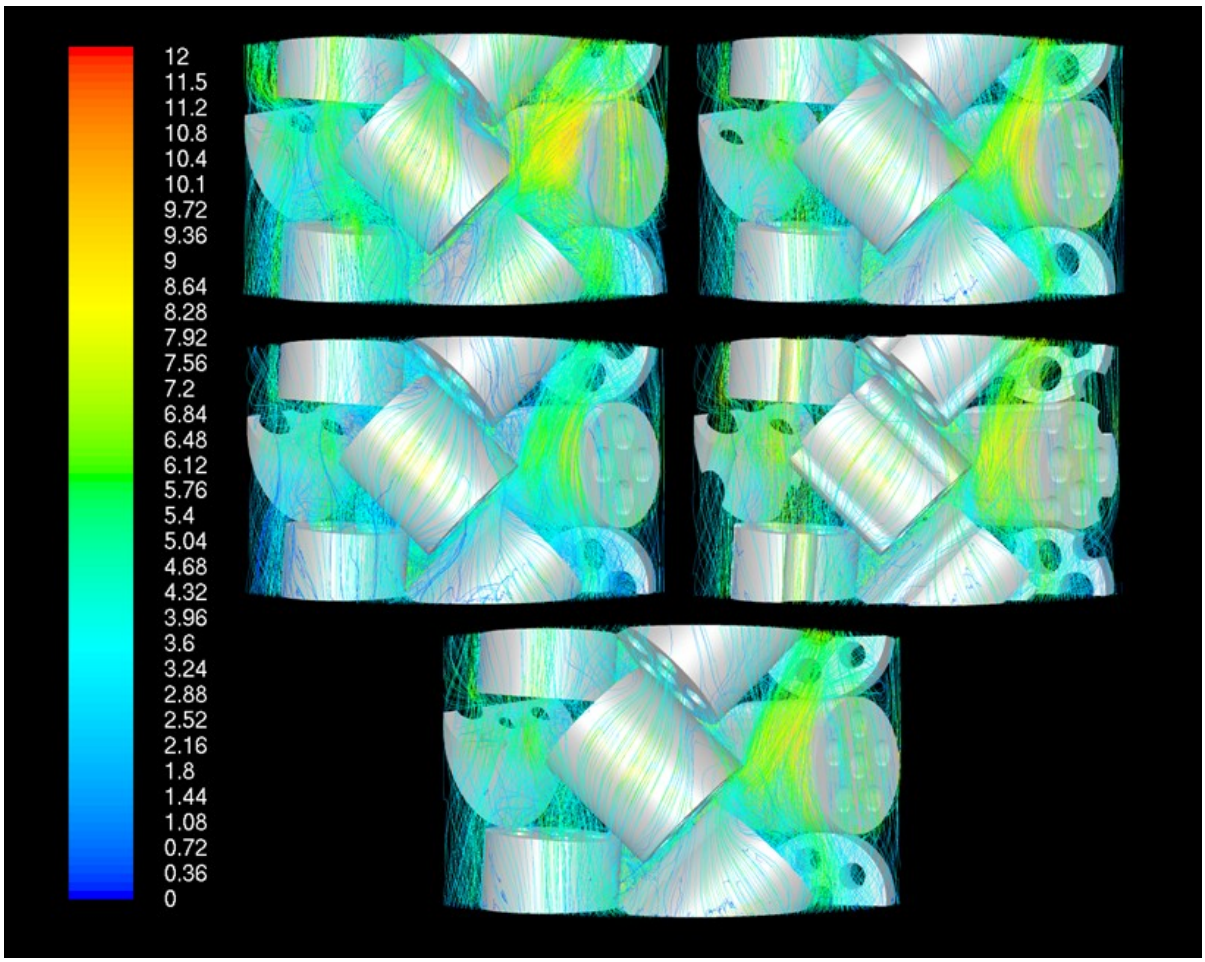

FIGURE 20: VELOCITY PATHLINES (M/S) COMPARISONS THROUGH REACTOR WEDGE.

Figure 21 compares the velocity pathlines over and through particle 1 and into the test particle. For the 1-hole case, much of the flow hits the bottom of the test particle and is deflected in a radial direction. In general, the more holes there are, the more likely it is that flow is pulled through the holes instead of being deflected radially. This effect has its advantages and disadvantages. Flow going through the holes is kept close the particle's surface where the reaction takes place. As a result of this, not only do holes create more surface area, but they help redirect flow which maximizes the utilization of this surface

area. However, the addition of more holes results in less radial flow. The reduction of radial flow reduces radial heat transfer and increases the tube wall temperature.

The tube wall temperature not only increases with increasing void fraction but also depends on the configuration of the holes. For example, the difference in tube wall temperature from the 3-hole and 6-hole cases is greater than 10 K despite the fact that both cases have the same void fraction. Since there are double the number of holes in the 6-hole case and these holes are spread out over the bottom surface of the particle, the chances of flow being "captured" by a hole is increased.

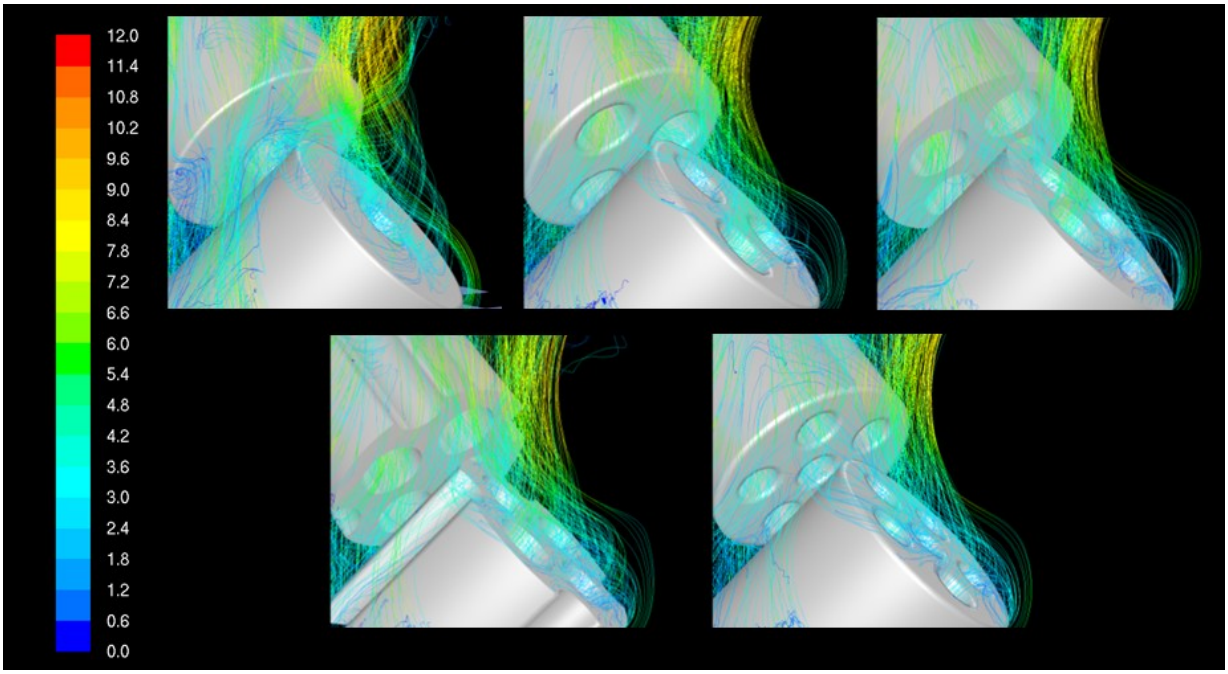

FIGURE 21: VELOCITY PATHLINE (M/S) COMPARISONS THROUGH PARTICLE 1 AND TEST PARTICLE HOLES.

Figure 22 and Figure 23 are further proof that the grooves channel the flow along the test particle. The velocity pathlines for the 4-hole case hit the bottom edge of the test particle and are deflected away from the particle. However, the velocity pathlines for the 4-hole with grooves case split into two directions: some of the flow is deflected like the 4-hole case while the rest is funneled along the groove (Figure 23). The funneling created by the grooves helps keep flow close to the surface where the reaction is occurring.

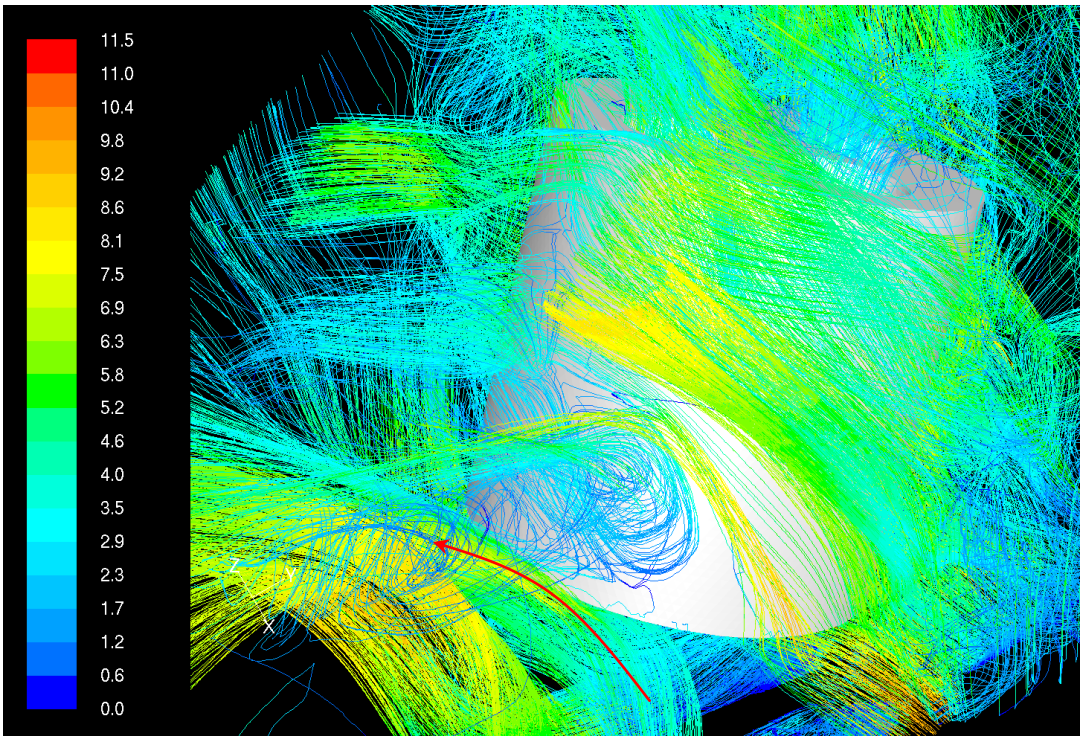

FIGURE 22: VELOCITY PATHLINES (M/S) IN 4-HOLE CASE.

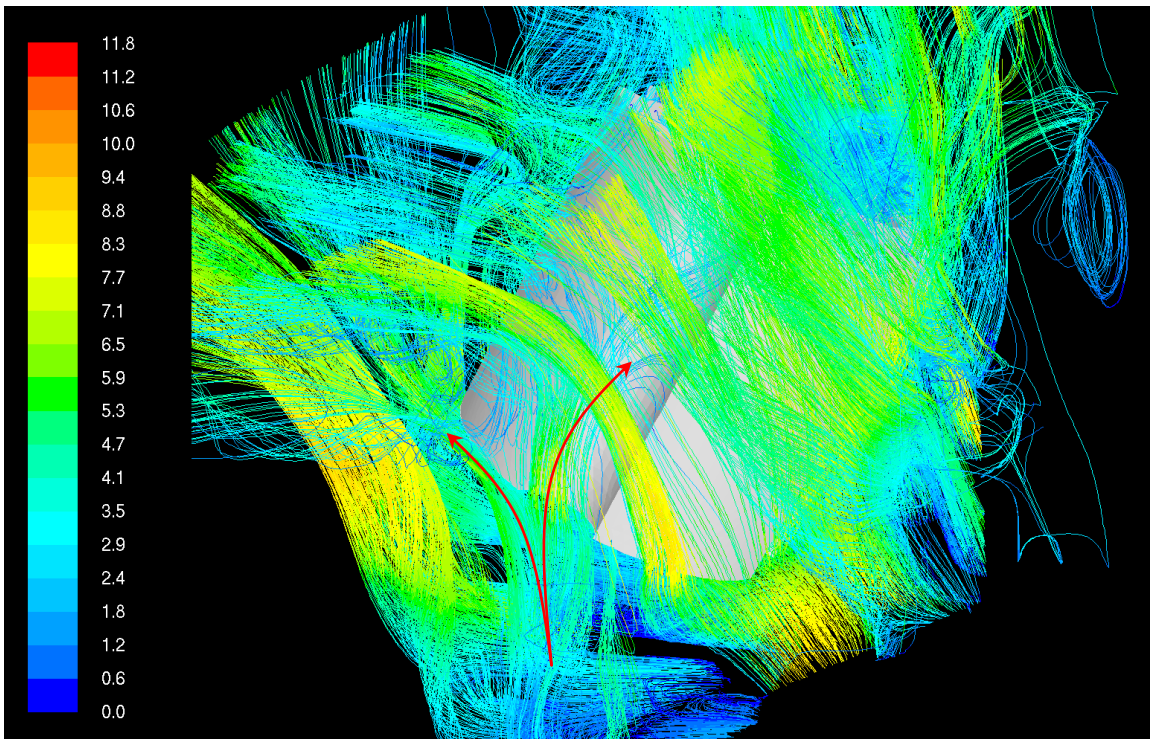

FIGURE 23: VELOCITY PATHLINES (M/S) IN 4-HOLE WITH GROOVES CASE.

METHANE CONVERSION COMPARISONS

Figure 24 shows the methane mass fraction gradients for each of the five catalyst geometries. The location of the holes in each of the cases has a significant impact on how effectively the holes are utilized. In the 1-hole case, the hole is at the center of the particle. Below the test particle, there is another particle blocking flow (not shown). Since the single hole is in the center of the test particle, it is difficult for flow to enter the hole and replenish it with methane. In the 6-hole case, the larger number of holes results in less tortuous flow and the holes are utilized more effectively.

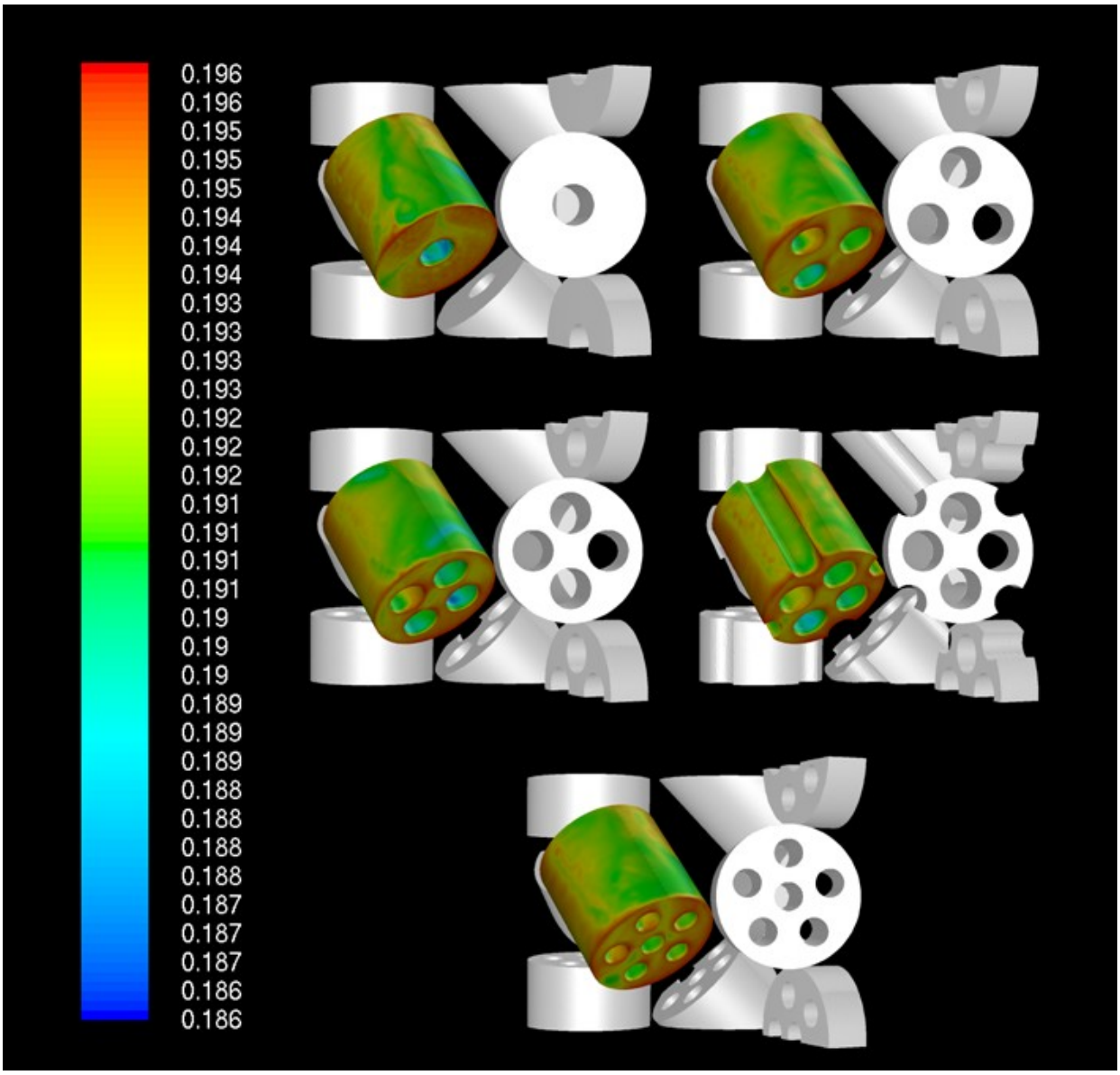

FIGURE 24: TEST PARTICLE METHANE MASS FRACTION GRADIENT COMPARISONS (PARTICLES 3 AND 7 REMOVED).

Figure 25 compares the methane conversion gradients between geometries for a cross-section of the reactor wedge. It can be seen that the methane does not diffuse deep into the particle. This diffusion limitation has been seen in previous research as well. In one paper, the reaction was found to occur within 3-5% of the particle radius from the surface (Pedernera, Pina, Borio, & Bucala, 2003). This can be more clearly seen in Figure 26. Since the reaction occurs very close to the surface, the addition of holes and grooves increases the surface area and thus the area available for reaction.

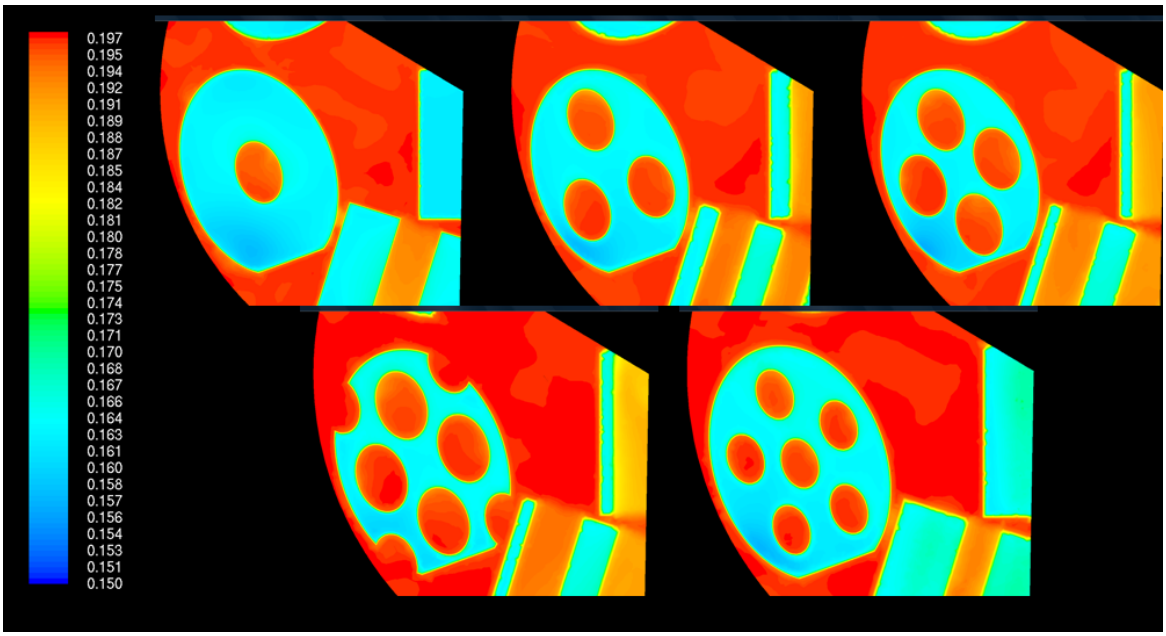

FIGURE 25: CROSS-SECTIONAL REACTOR WEDGE COMPARISONS OF METHANE CONVERSION GRADIENT.

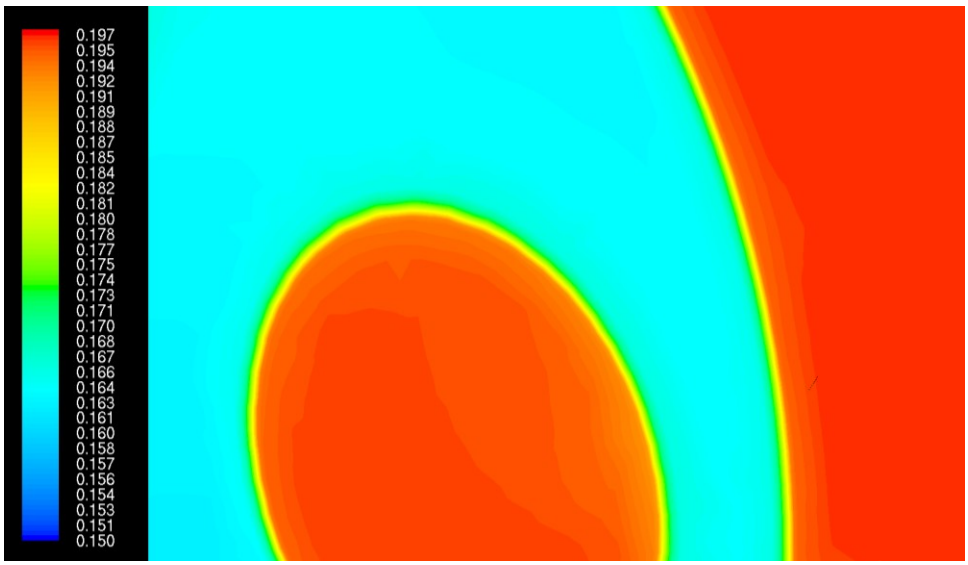

FIGURE 26: CLOSE-UP OF METHANE MASS FRACTION CROSS-SECTION (3-HOLE).

REACTION RATE COMPARISONS

The test particle rates of reaction for reactions 1 and 3 are shown in Figure 27 and Figure 28, respectively. The intensity of the reaction rates closely follows the intensity of the temperature hot spot (see Figure 8). This is expected since reactions 1 and 3 are highly endothermic. Due to the endothermicity of these reactions, high temperature will drive the reaction forward. This is why the reaction rate is the highest where the temperature is the highest.

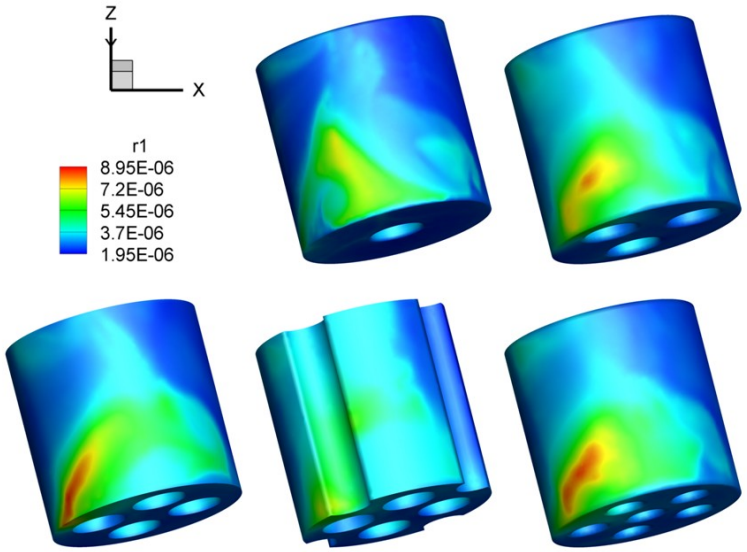

FIGURE 27: TEST PARTICLE RATE OF REACTION 1 CONTOUR COMPARISONS.

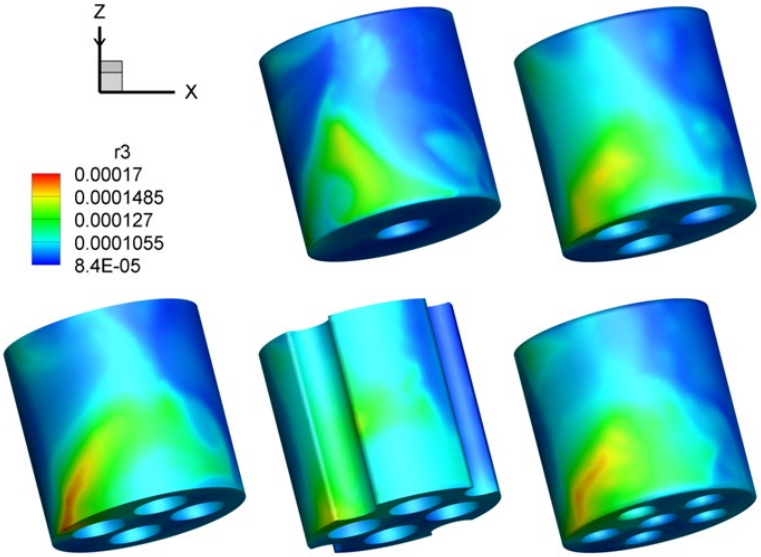

FIGURE 28: TEST PARTICLE RATE OF REACTION 3 CONTOUR COMPARISONS.

FLOW PATTERNS AND SURFACE CONTOURS

The effects of flow on temperature, methane mass fraction, and reaction rates were examined closely. A side-by-side comparison of the various surface contours can be seen in Figure 29. Since the first and third reactions are endothermic, the location of the temperature hotspot and highest reaction rates correspond well.

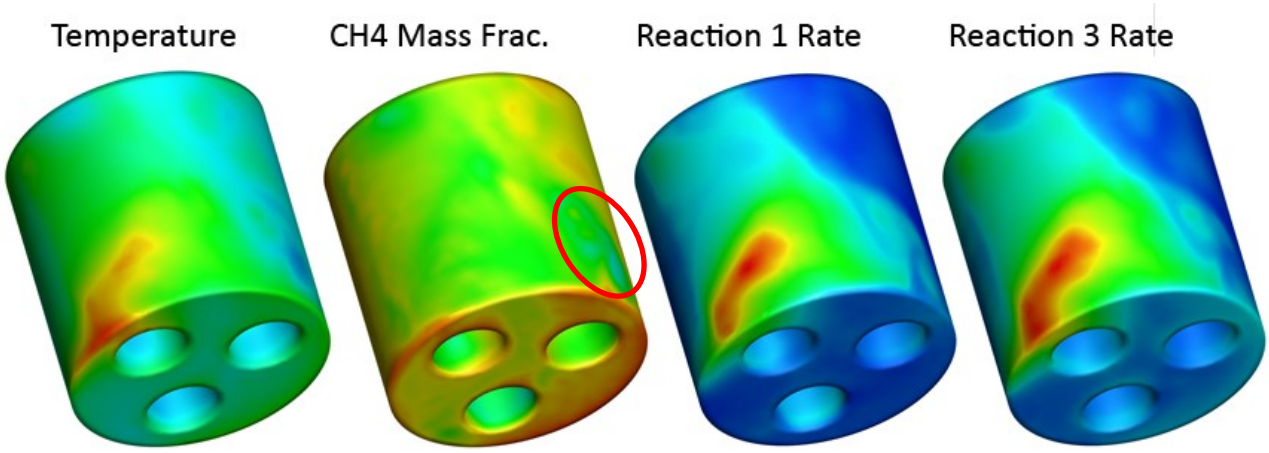

FIGURE 29: 3-HOLE SURFACE CONTOUR COMPARISONS.

Since both reactions consume methane, the expected location of the minimum methane mass fraction would be where the reaction occurs the most. However, this is not the case. The minimum methane mass fraction actually occurs slightly to the right of the maximum reaction rate (circled in red). In order to better understand why this was occurring, it was necessary to examine the flow patterns near the test particle.

Figure 30 is a close-up of the test particle in the 3-hole case. Two factors influence the temperature contour on the test particle: distance from the tube wall and the velocity of the fluid passing over the particle's surface. On the far right of Figure 30, the temperature is quite low. Moving further along the surface, the temperature starts to increase as the distance from the tube wall starts to decrease. However, near the tube wall the velocity of the fluid starts to increase. The region with the most intense velocity has a slightly lower temperature (circled in red). It can also be seen that at the location of the hotspot, the fluid is quite stagnant. Thus, the distance from the tube wall and the velocity of the fluid passing over the surface determine where the hotspot occurs.

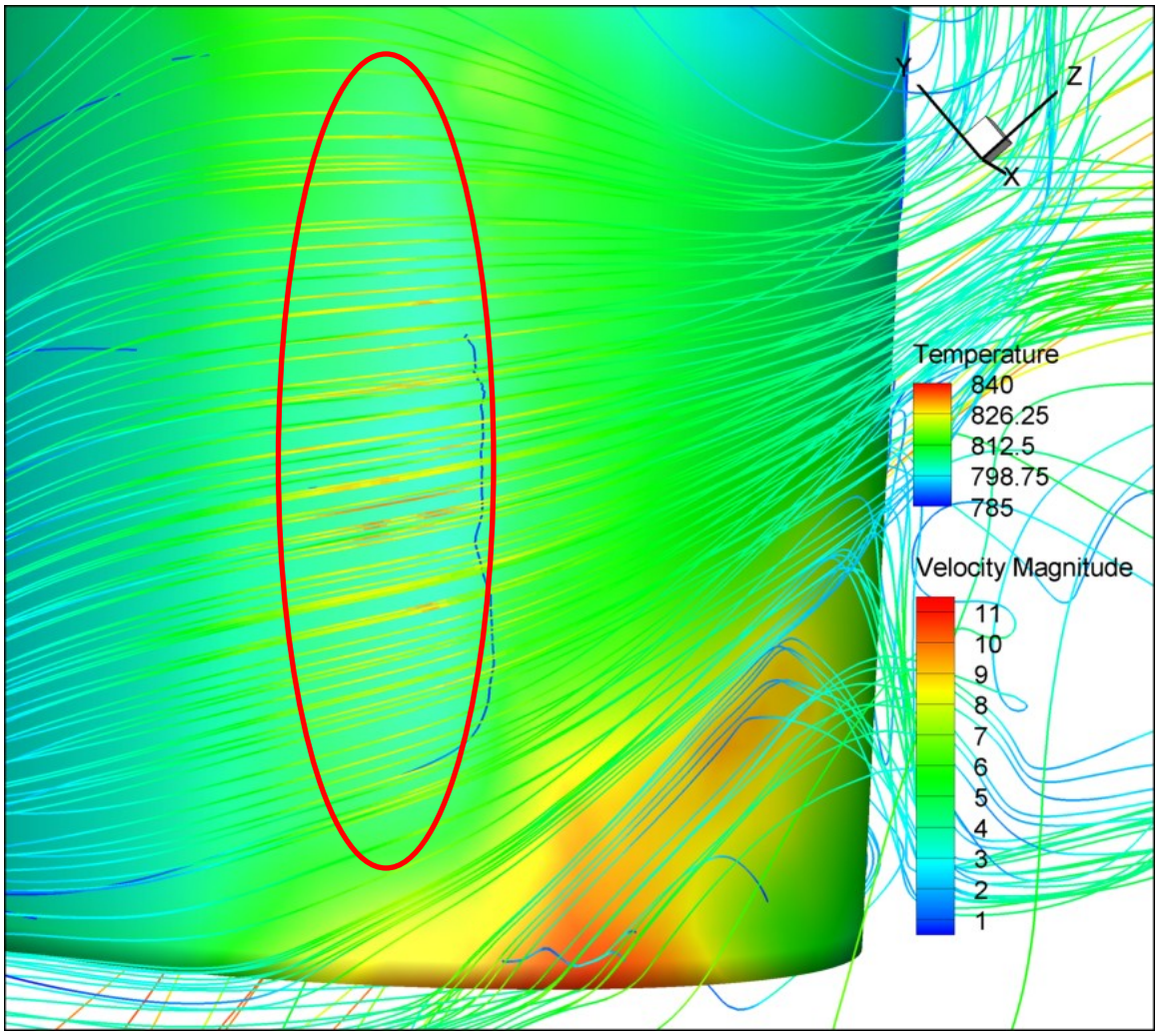

FIGURE 30: TEMPERATURE CONTOURS WITH VELOCITY PATHLINES OVERLAYED (3-HOLE).

While the contours for temperature and reaction rates closely match, the methane mass fractions do not match up as well. Intuition would suggest that areas of low methane would be found where the temperature and reaction rates are the highest since methane is consumed in the reaction. However, this is not the case.

Figure 31 shows the surface methane mass fraction on the 3-hole test particle. Velocity pathlines are overlaid. This view displays a side of the test particle that is further from the tube wall than Figure 30. The minimum surface methane mass fraction was found in an area of highly stagnant flow (circled in red). The slow circular flow seen in Figure 31 suggests that methane is hardly being replenished. In addition to being starved of reactant, this location is further from the hot tube wall. The combination of these two factors results in an area with little reaction and very little methane. This explains why the minimum methane mass fraction was not found in the same area as the hotspot.

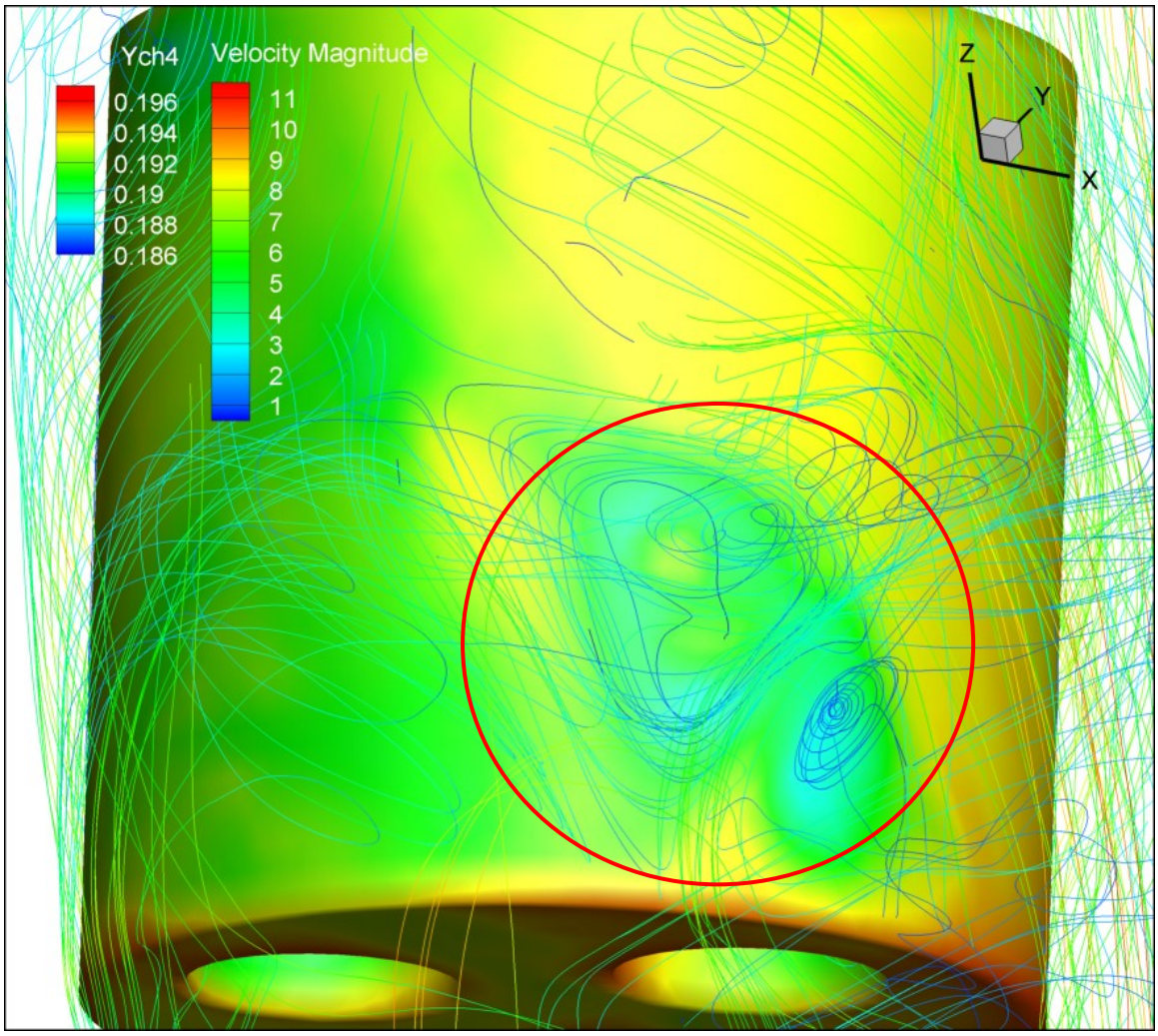

FIGURE 31: METHANE CONVERSION CONTOURS FOR 3-HOLE TEST PARTICLE WITH OVERLAYED PATHLINES.

CONCLUSIONS AND RECOMMENDATIONS

Steam methane reforming is a widely-used process to convert methane into a mixture of hydrogen and carbon monoxide (syngas). Due to its maturity, high efficiency, and relatively low cost, steam reforming is considered a viable option for supporting a future hydrogen economy. A conventional steam reformer consists of several hundred fixed-bed reactor tubes filled with supported nickel catalyst particles, which can vary in size and geometry.

The goal of this project was to compare multi-holed cylindrical catalyst geometries using computational fluid dynamics in order to propose recommendations for better catalyst particle design, which can help lead to more efficient steam methane reforming technology. This project expanded upon the previously studied 1-hole and 4-hole geometries by adding an extended range of catalyst geometries: 3-hole, 6-hole, 4-hole with vertical grooves.

The results for the wall segment as a whole were studied. The pressure drop was specified as 3,376 Pa/m for all the cases, and the pressure drop stayed close to the set value for each case. As expected, as the void fraction increased, the mass flow rate increased. The average temperature of the exiting gas decreased as the void fraction increased because more mass was flowing through the tube. The average reactor tube wall temperature generally increased as the void fraction increased. However, the average temperature for the 6-hole case was more than 10 K hotter than the 3-hole case that had the same void fraction. This was due to variations in flow; in particular the 6-hole case had less tortuous flow which resulted in less effective radial heat transfer.

Next, the results for the test particle itself were studied. In general, as the surface area of the particle increased, so did the amount of reaction, as evidenced by the reaction rates and heat sinks. Since the dominant reactions in steam methane reforming are endothermic, a higher heat sink means more reaction is occurring. The particle surface heat flux was examined to make sure that the energy balance was correct. The amount of heat flux on the particle surface should equal the amount of heat the particle takes in due to the reaction, and for these simulations the heat sink and heat flux were approximately equal.

Thus, it was concluded that both the 4-hole with grooves and 6-hole geometries offered the highest surface area and reaction rates while still maintaining a uniform temperature profile. However, the 6-hole case had a smaller void fraction than the 4-hole with grooves. As a result, the 6-hole case had lower mass flow rates for the set pressure drop. In addition, the 6-hole case had a significantly higher

tube wall temperature of 1070 K compared to the 4-hole with groove's temperature of 1062 K. The 1-hole, 3-hole, and 4-hole cases had even lower tube wall temperatures (1055.6, 1058.4 and 1057.7 K respectively). However, the lesser-holed cases had significantly less surface area and void fraction when compared with the 4-hole with grooves case. Overall, the 4-hole with grooves geometry offers high surface area for reaction, high void fraction for low pressure drops, and uniform temperature within the reactor at the cost of a slightly higher tube wall temperature.

An aspect of catalyst design that was not examined in this paper but that should be taken into consideration for future study is the strength of the geometries. Over time, catalyst particles get crushed inside the reactor bed and eventually clog the reactor. Thus, an optimal catalyst design would have high strength in addition to the characteristics discussed in this paper.

REFERENCES

Broadhurst, P., & Abbott, P. (2002). *Improving hydrogen plant performance: Part II.* Retrieved February 18, 2010, from Johnson Matthey Catalysts: http://www.jmcatalysts.com

Bruno, S., Guillermo, F., & Gonzalez, M. (1988). Effect of the geometric characteristics of commercial catalysts for steam reforming. *The Chemical Engineering Journal , 39*, 147-156.

Dixon, A.G. (2009). Private communication.

Dixon, A., Nijemeisland, M., & Stitt, E. (2006). Packed tubular reactor modeling and catalyst design using computational fluid dynamics. *Advances in Chemical Engineering , 31*, 307-389.

Dixon, A., Taskin, M., Nijemeisland, M., & Stitt, E. (2008). Wall-to-particle heat transfer in steam reformer tubes: CFD comparison of catalyst particles. *Chemical Engineering Science , 63*, 2219-2224.

Dixon, A., Taskin, M., Stitt, E., & Nijemeisland, M. (2007). 3D CFD simulations of steam reforming with resolved intraparticle reaction and gradients. *Chemical Engineering Science , 62*, 4963-4966.

Hou, K., & Hughes, R. (2001). The kinetics of methane steam reforming over a Ni/a-Al2O catalyst. *Chemical Engineering Journal* , 311-328.

Hydrogen production - steam methane reforming (SMR). (n.d.). Retrieved February 18, 2010, from New York State Energy Research and Development Authority: http://www.getenergysmart.org

Kagyrmanova, A., Zolotarskii, I., Smirnov, E., & Vernikovskaya, N. (2007). Optimum dimensions of shaped steam reforming catalysts. *Chemical Engineering Journal , 134*, 228-234.

Kagyrmanova, A., Zolotarskii, I., Vernikovskaya, N., Smirnov, E., Kuz'min, V., & Chumakova, N. (2006). Modeling of steam reforming of natural gas using catalysts with grains of complex shapes. *Theoretical Foundations of Chemical Engineering , 40*, 155-167.

Katalco 57-series. (n.d.). *Catalyst Characteristics* . Johnson Matthey Catalysts.

Kolaczkowski, S., Chao, R., Awdry, S., & Smith, A. (2007). Application of a CFD code (Fluent) to formulate models of catalytic gas phase reactions in porous catalyst pellets. *Chemical Engineering Research and Design , 85*, 1539-1552.

Menter, F. (1993). Zonal two equation k-ω turbulence models for aerodynamic flows. *AIAA Paper* , 93-2906.

Menter, F., Kuntz, M., & Langtry, R. (2003). Ten years of industrial experience with the SST turbulence model. *Proc of the 4th International Symposium on Turbulence, Heat and Mass Transfer*, 625-632.

Nijemeisland, M. (2003). *Influences of catalyst particle geometry on fixed bed reactor near-wall heat transfer using CFD* (Doctoral thesis, Worcester Polytechnic Institute). Retrieved from http://www.wpi.edu/Pubs/ETD/Available/etd-0130103-181607/unrestricted/01mnijemeisland.pdf

Nijemeisland, M., & Dixon, A. (2004). CFD study of fluid flow and wall heat transfer in a fixed bed of spheres. *AIChE Journal , 50*, 906-921.

Nijemeisland, M., & Dixon, A. (2001). Comparison of CFD simulations to experiment for convective heat transfer in a gas-solid fixed bed. *Chemical Engineering Journal , 82*, 231-246.

Nijemeisland, M., Dixon, A., & Stitt, E. (2004). Catalyst design by CFD for heat transfer and reaction in steam reforming. *Chemical Engineering Science , 59*, 5185-5191.

Pedernera, M., Pina, J., Borio, D., & Bucala, V. (2003). Use of a heterogeneous two-dimensional model to improve the primary steam reformer performance. *Chemical Engineering Journal , 94*, 29-40.

Product data. (2007). *Primary Steam Reforming Catalyst: Rare Earth Promoted Nickel Oxide Technology* . BASF Catalysts LLC.

Sie, S., & Krishna, R. (1998). Process design and scale up: II. Catalyst design strategy. *Reviews in Chemical Engineering , 14* (3), 159-202.

Stitt, E. (2005). Substainable strategies for the upgrading of natural gas. *NATO Science Series II Mathematics, Physics, & Chemistry , 191*, 185-216.

Taskin, M. (2007). *CFD simulation of transport and reaction in cylindrical catalyst particles* (Doctoral thesis, Worcester Polytechnic Institute). Retrieved from http://www.wpi.edu/Pubs/ETD/Available/etd-081507-135028/unrestricted/Taskin01.pdf

Troupel, M.E. (2009). *CFD study of the intra and inter particles transport phenomena in a fixed-bed reactor* (Master's thesis, Worcester Polytechnic Institute). Retrieved from http://www.wpi.edu/Pubs/ETD/Available/etd-052809-145316/restricted/atroupel.pdf

APPENDIX A: PARTICLE PLACEMENT TABLE

Particle	Orientation 1b	Orientation 2	Orientation 3
1	R +45 +x T -1.45 +x R +40 +z	R +90 +y T -1.42 +x T +1 +z R +30 +z	R +90 +x T -1.42 +x T +1 +z R +30 +z
2	R -45 +x T -1.45 +x T +1 +z R +20 +z	R +90 +x R +30 +z T +1 +z T +0.5 +y T -1.17 +x	h = 0.98 T -1.48 +x R +45 +z
3	**1** C +2 +z	h = 0.98 T -1.48 +x R +5 +z	**2** C +2 +z
4	R +5 +x T -1.48 +x R -9 +z	**3** C +2 +z	R +45 +x T -1.45 +x T +1 +z R -25 +z
5	**4** C +2 +z	R +90 +x T -1.42 +x R +55 +z	R -45 +x T -1.45 +x R -5 +z
6	R +90 +y T -1.42 +y R +5 +z	**5** C +2 +z	**5** C +2 +z
7	**6** C +2 +z	h = 0.98 T -1.48 +x T +1 +z R +75 +z	R +45 +x T -1.45 +x T +1 +z R +85 +z
8	R +90 +x T -1.42 +y T +1 +z R -17.5 +z	h = 0.98 T +1 +z T -0.2 +y T -0.35 +x	R -45 +x T -1.45 +x R +105 +z
9	R +45 +x T -1.45 +x T +1 +z R -40 +z	R +90 +x R +40 +z T -0.18 +y T -0.25 +x	**8** C +2 +z
10	R +90 +y T -0.25 +x	**9** C +2 +z	r = 0.49 R +90 +y T +1 +z T -0.25 +x
11	**10** C +2 +z	R +45 +x T -1.45 +x R -50 +z	R +90 +x R +30 +z T -0.25 +x T -0.25 +y
12	R +90 +x T +1 +z T -0.35 +y T +0.2 +x	**11** C +2 +z	**11** C +2 +z

R = rotate, T = translate, C = copy, h = adjust height to, r = adjust radius to. Rotations are in degrees, translations in inches. Based on particle of 1 inch diameter, 1 inch height (Nijemeisland, 2003).

APPENDIX B: SAMPLE GAMBIT JOURNAL FILE

```
/ Identifier "3-HOLE-WITH-BL"
identifier name "3-HOLE-WITH-BL" new nosaveprevious
solver select "FLUENT 5/6"
reset
volume create "cylinder" height 2 radius1 2 radius2 2 radius3 2 offset 0 0 1 \
  zaxis frustum
volume create "part" height 1 radius1 0.5 radius3 0.5 zaxis frustum
volume create "hole1" height 1 radius1 0.1434 radius3 0.1434 zaxis frustum
volume create "hole2" height 1 radius1 0.1434 radius3 0.1434 zaxis frustum
volume create "hole3" height 1 radius1 0.1434 radius3 0.1434 zaxis frustum
volume move "hole1" offset 0 0.26 0
volume move "hole2" offset 0 0.26 0
volume move "hole2" dangle 120 vector 0 0 1 origin 0 0 0
volume move "hole3" offset 0 0.26 0
volume move "hole3" dangle -120 vector 0 0 1 origin 0 0 0
volume subtract "part" volumes "hole1"
volume subtract "part" volumes "hole2"
volume subtract "part" volumes "hole3"
volume copy "part" to "part1"
volume move "part1" dangle 45 vector 1 0 0 origin 0 0 0
volume move "part1" offset -1.45 0 0
volume move "part1" dangle 40 vector 0 0 1 origin 0 0 0
volume copy "part" to "part2"
volume move "part2" dangle -45 vector 1 0 0 origin 0 0 0
volume move "part2" offset -1.45 0 0
volume move "part2" dangle 20 vector 0 0 1 origin 0 0 0
volume move "part2" offset 0 0 1
volume copy "part1" to "part3"
volume move "part3" offset 0 0 2
volume copy "part" to "part4"
volume move "part4" dangle 5 vector 1 0 0 origin 0 0 0
volume move "part4" offset -1.48 0 0
volume move "part4" dangle -9 vector 0 0 1 origin 0 0 0
volume copy "part4" to "part5"
volume move "part5" offset 0 0 2
volume copy "part" to "part6"
volume move "part6" dangle 90 vector 0 1 0 origin 0 0 0
volume move "part6" offset 0 -1.42 0
volume move "part6" dangle 5 vector 0 0 1 origin 0 0 0
volume copy "part6" to "part7"
volume move "part7" offset 0 0 2
volume copy "part" to "part8"
volume move "part8" dangle 90 vector 1 0 0 origin 0 0 0
volume move "part8" offset 0 0 1
volume move "part8" offset 0 -1.42 0
volume move "part8" dangle -17.5 vector 0 0 1 origin 0 0 0
volume copy "part1" to "part9"
volume move "part9" offset 0 0 1
volume move "part9" dangle -40 vector 0 0 1 origin 0 0 0
volume move "part9" dangle -40 vector 0 0 1 origin 0 0 0
volume copy "part" to "part10"
volume move "part10" dangle -45 vector 0 1 0 origin 0 0 0
volume move "part10" offset -0.25 0 0
volume copy "part10" to "part11"
volume move "part11" offset 0 0 2
volume copy "part" to "part12"
volume move "part12" dangle 90 vector 1 0 0 origin 0 0 0
volume move "part12" offset 0 0 1
volume move "part12" offset 0.2 0 0
```

```
volume move "part12" offset 0 -0.35 0
volume delete "part" lowertopology
volume create "b1" width 3 depth 3 height 4 offset 1.5 1.5 2 brick
volume move "b1" offset 0 0 -1
volume copy "b1" to "b2"
volume move "b2" dangle 60 vector 0 0 1 origin 0 0 0
volume copy "b1" to "b3"
volume move "b3" dangle -90 vector 0 0 1 origin 0 0 0
volume copy "b1" to "b4"
volume move "b4" offset -3 0 -3
volume copy "b4" to "b5"
volume move "b5" offset 0 -3 0
volume copy "b5" "b4" to "b6" "tool"
volume move "b6" "tool" offset 0 0 6
volume unite volumes "tool" "b6" "b4" "b5" "b2" "b1" "b3"
/ Modification to W geometry
volume move "tool" dangle -1 vector 0 0 1 origin 0 0 0
volume move "part1" "part2" "part3" "part4" "part5" "part6" "part7" "part8" \
  "part9" "part10" "part11" "part12" offset 0 0 0.04
/ Trim cylinder and the eleven particles that stick out of the segment
volume subtract "cylinder" volumes "tool" keeptool
volume subtract "part7" volumes "tool" keeptool
volume subtract "part3" volumes "tool" keeptool
volume subtract "part11" volumes "tool" keeptool
volume subtract "part5" volumes "tool" keeptool
volume subtract "part4" volumes "tool" keeptool
volume subtract "part1" volumes "tool" keeptool
volume subtract "part10" volumes "tool" keeptool
volume subtract "part6" volumes "tool" keeptool
volume subtract "part12" volumes "tool" keeptool
volume subtract "part8" volumes "tool" keeptool
volume subtract "part9" volumes "tool"
/ Subtract particles from cylinder and connect back the faces (28 pairs)
volume subtract "cylinder" volumes "part1" keeptool
volume subtract "cylinder" volumes "part2" keeptool
volume subtract "cylinder" volumes "part3" keeptool
volume subtract "cylinder" volumes "part4" keeptool
volume subtract "cylinder" volumes "part5" keeptool
volume subtract "cylinder" volumes "part6" keeptool
volume subtract "cylinder" volumes "part7" keeptool
volume subtract "cylinder" volumes "part8" keeptool
volume subtract "cylinder" volumes "part9" keeptool
volume subtract "cylinder" volumes "part10" keeptool
volume subtract "cylinder" volumes "part11" keeptool
volume subtract "cylinder" volumes "part12" keeptool
/ Label the two parts of the fluid that are disconnected
volume modify "volume.15" label "fluid-part11-hole3"
volume modify "volume.16" label "fluid-part11-hole2"
/ Label top, bottom, and cylinder
face modify "face.467" label "bottom"
face modify "face.2" label "cylinder-wall"
face modify "face.484" label "top"
/ Connect particle 1 fluid faces and label all particle 1 faces
face connect "face.18" "face.384" real
face connect "face.20" "face.385" real
face connect "face.285" "face.380" real
face connect "face.16" "face.382" real
face connect "face.17" "face.383" real
face connect "face.15" "face.381" real
face modify "face.18" label "part01-1"
face modify "face.20" label "part01-2"
face modify "face.285" label "part01-3"
face modify "face.16" label "part01-hole1"
```

```
face modify "face.17" label "part01-hole2"
face modify "face.15" label "part01-hole3"
face modify "face.284" label "part01-bottom"
face modify "face.386" label "bottom-part01-hole1"
face modify "face.388" label "bottom-part01-hole2"
face modify "face.387" label "bottom-part01-hole3"
/ Connect particle 3 fluid faces and label all particle 3 faces
face connect "face.30" "face.400" real
face connect "face.200" "face.396" real
face connect "face.28" "face.398" real
face connect "face.29" "face.399" real
face connect "face.27" "face.397" real
face modify "face.30" label "part03-1"
face modify "face.200" label "part03-2"
face modify "face.28" label "part03-hole1"
face modify "face.29" label "part03-hole2"
face modify "face.27" label "part03-hole3"
face modify "face.201" label "part03-top"
face modify "face.401" label "top-part03-hole1"
face modify "face.403" label "top-part03-hole2"
face modify "face.402" label "top-part03-hole3"
/ Connect particle 2 fluid faces and label all particle 2 faces
face connect "face.24" "face.392" real
face connect "face.26" "face.394" real
face connect "face.25" "face.393" real
face connect "face.22" "face.390" real
face connect "face.23" "face.391" real
face connect "face.21" "face.389" real
face modify "face.24" label "part02-1"
face modify "face.26" label "part02-2"
face modify "face.25" label "part02-3"
face modify "face.22" label "part02-hole1"
face modify "face.23" label "part02-hole2"
face modify "face.21" label "part02-hole3"
/ Connect particle 4 fluid faces and label all particle 4 faces
face connect "face.36" "face.408" real
face connect "face.38" "face.409" real
face connect "face.34" "face.406" real
face connect "face.35" "face.407" real
face connect "face.33" "face.405" real
face modify "face.36" label "part04-1"
face modify "face.38" label "part04-2"
face modify "face.34" label "part04-hole1"
face modify "face.35" label "part04-hole2"
face modify "face.33" label "part04-hole3"
face modify "face.264" label "part04-bottom"
face modify "face.411" label "bottom-part04-hole1"
face modify "face.412" label "bottom-part04-hole2"
face modify "face.1" label "bottom-part04-hole3"
/ Connect particle 5 fluid faces and label all particle 5 faces
face connect "face.42" "face.417" real
face connect "face.43" "face.418" real
face connect "face.40" "face.415" real
face connect "face.41" "face.416" real
face connect "face.39" "face.414" real
face modify "face.42" label "part05-1"
face modify "face.43" label "part05-2"
face modify "face.40" label "part05-hole1"
face modify "face.41" label "part05-hole2"
face modify "face.39" label "part05-hole3"
face modify "face.244" label "part05-top"
face modify "face.420" label "top-part05-hole1"
face modify "face.421" label "top-part05-hole2"
```

```
face modify "face.158" label "top-part05-hole3"
/ Connect particle 9 fluid faces and label all particle 9 faces
face connect "face.66" "face.453" real
face connect "face.68" "face.454" real
face connect "face.63" "face.451" real
face connect "face.64" "face.452" real
face connect "face.378" "face.450" real
face modify "face.66" label "part09-1"
face modify "face.68" label "part09-2"
face modify "face.64" label "part09-hole1"
face modify "face.378" label "part09-hole2"
face modify "face.63" label "part09-hole3"
face modify "face.377" label "part09-sym1"
face modify "face.455" label "sym1-part09-hole1"
face modify "face.147" label "sym1-part09-hole3"
/ Connect particle 6 fluid faces and label all particle 6 faces
face connect "face.48" "face.427" real
face connect "face.49" "face.428" real
face connect "face.331" "face.425" real
face connect "face.46" "face.426" real
face modify "face.48" label "part06-1"
face modify "face.49" label "part06-2"
face modify "face.331" label "part06-hole1"
face modify "face.46" label "part06-hole2"
face modify "face.332" label "part06-sym2"
face modify "face.429" label "sym2-part06-hole1"
face modify "face.430" label "sym2-part06-hole2"
face modify "face.320" label "part06-bottom-1"
face modify "face.330" label "part06-bottom-2"
/ Connect particle 7 fluid faces and label all particle 7 faces
face connect "face.54" "face.437" real
face connect "face.55" "face.438" real
face connect "face.178" "face.435" real
face connect "face.51" "face.436" real
face modify "face.54" label "part07-1"
face modify "face.55" label "part07-2"
face modify "face.178" label "part07-hole1"
face modify "face.51" label "part07-hole2"
face modify "face.180" label "part07-top-1"
face modify "face.175" label "part07-top-2"
face modify "face.179" label "part07-sym2"
face modify "face.431" label "sym2-part07-hole1"
face modify "face.440" label "sym2-part07-hole2"
/ Connect particle 8 fluid faces and label all particle 8 faces
face connect "face.60" "face.446" real
face connect "face.62" "face.448" real
face connect "face.61" "face.447" real
face connect "face.58" "face.444" real
face connect "face.59" "face.445" real
face modify "face.60" label "part08-1"
face modify "face.62" label "part08-2"
face modify "face.61" label "part08-3"
face modify "face.58" label "part08-hole1"
face modify "face.59" label "part08-hole2"
/ Connect particle 10 fluid faces and label all particle 10 faces
face connect "face.72" "face.465" real
face connect "face.74" "face.466" real
face connect "face.70" "face.464" real
face connect "face.310" "face.462" real
face connect "face.69" "face.463" real
face modify "face.72" label "part10-1"
face modify "face.74" label "part10-2"
face modify "face.70" label "part10-hole1"
```

```
face modify "face.310" label "part10-hole2"
face modify "face.69" label "part10-hole3"
face modify "face.307" label "part10-sym1-1"
face modify "face.309" label "part10-sym1-2"
face modify "face.308" label "part10-sym2-1"
face modify "face.306" label "part10-sym2-2"
face modify "face.305" label "part10-bottom"
face modify "face.456" label "sym1-part10-hole3"
face modify "face.470" label "sym2-part10-hole3"
face modify "face.468" label "bottom-part10-hole1"
face modify "face.469" label "bottom-part10-hole2"
face modify "face.410" label "bottom-part10-hole3"
/ Connect particle 12 fluid faces and label all particle 12 faces
face connect "face.353" "face.492" real
face connect "face.355" "face.491" real
face connect "face.354" "face.490" real
face connect "face.82" "face.493" real
face modify "face.353" label "part12-1"
face modify "face.355" label "part12-2"
face modify "face.354" label "part12-3"
face modify "face.82" label "part12-hole1"
face modify "face.341" label "part12-sym1"
face modify "face.356" label "part12-sym2-1"
face modify "face.352" label "part12-sym2-2"
face modify "face.494" label "sym1-part12-hole1"
/ Connect particle 11 fluid faces and label all particle 11 faces
face connect "face.222" "face.477" real
face connect "face.221" "face.476" real
face connect "face.77" "face.480" real
face connect "face.75" "face.479" real
face modify "face.222" label "part11-1"
face modify "face.221" label "part11-2"
face modify "face.77" label "part11-hole2"
face modify "face.75" label "part11-hole3"
face modify "face.210" label "part11-sym1"
face modify "face.441" label "top-part11-hole2"
face modify "face.486" label "top-part11-hole3"
face modify "face.472" label "sym2-part11-hole3"
face modify "face.483" label "sym1-part11-hole2"
/ Connect faces that require to be virtual
face connect "face.376" "face.443" virtual
face connect "face.223" "face.478" virtual
/ Label faces that became virtual
face modify "v_face.500" label "part08-hole3"
face modify "v_face.496" label "part08-sym2"
face modify "v_face.506" label "part11-hole1"
face modify "v_face.501" label "part11-top"
face modify "v_face.504" label "top-part11-hole1"
face modify "v_face.505" label "part11-sym2"
/ Label sides here, since they became virtual
face modify "face.481" label "sym1"
face modify "v_face.499" label "sym2"
/ Label volumes that changed to virtual
volume modify "v_volume.17" label "v_part8"
volume modify "v_volume.18" label "v_cylinder"
volume modify "v_volume.19" label "v_part11"
/
/END OF GEOMETRY SECTION, START OF MESHING
/
/ Link particle 5 top and particle 4 bottom
face link "bottom-part04-hole1" "top-part05-hole1" edges "edge.575" \
  "edge.520" vertices "vertex.426" "vertex.388" reverse periodic
face link "bottom-part04-hole2" "top-part05-hole2" edges "edge.576" \
```

```
  "edge.521" vertices "vertex.428" "vertex.390" reverse periodic
face link "bottom-part04-hole3" "top-part05-hole3" edges "edge.574" \
  "edge.519" vertices "vertex.427" "vertex.389" reverse periodic
face link "part04-bottom" "part05-top" edges "edge.577" "edge.575" "edge.576" \
  "edge.574" "edge.522" "edge.520" "edge.521" "edge.519" vertices \
  "vertex.425" "vertex.426" "vertex.428" "vertex.427" "vertex.387" \
  "vertex.388" "vertex.390" "vertex.389" reverse periodic
/ Link particle 3 top and particle 1 bottom
face link "bottom-part01-hole1" "top-part03-hole1" edges "edge.631" \
  "edge.397" vertices "vertex.463" "vertex.302" reverse periodic
face link "bottom-part01-hole2" "top-part03-hole2" edges "edge.632" \
  "edge.398" vertices "vertex.464" "vertex.303" reverse periodic
face link "bottom-part01-hole3" "top-part03-hole3" edges "edge.630" \
  "edge.396" vertices "vertex.465" "vertex.304" reverse periodic
face link "part01-bottom" "part03-top" edges "edge.633" "edge.632" "edge.630" \
  "edge.631" "edge.395" "edge.398" "edge.396" "edge.397" vertices \
  "vertex.466" "vertex.464" "vertex.465" "vertex.463" "vertex.305" \
  "vertex.303" "vertex.304" "vertex.302" reverse periodic
/ Link particle 7 top and particle 6 bottom
face link "part06-bottom-1" "part07-top-1" edges "edge.763" "edge.339" \
  vertices "vertex.554" "vertex.264" reverse periodic
face link "part06-bottom-2" "part07-top-2" edges "edge.761" "edge.336" \
  vertices "vertex.552" "vertex.262" reverse periodic
/ Link particle 11 top and particle 10 bottom
face link "bottom-part10-hole1" "top-part11-hole1" edges "edge.688" \
  "v_edge.1155" vertices "vertex.504" "v_vertex.832" reverse periodic
face link "bottom-part10-hole2" "top-part11-hole2" edges "edge.1082" \
  "edge.466" vertices "vertex.507" "vertex.351" reverse periodic
face link "bottom-part10-hole3" "top-part11-hole3" edges "edge.689" \
  "edge.1125" vertices "vertex.503" "vertex.347" reverse periodic
face link "part10-bottom" "part11-top" edges "edge.692" "edge.688" "edge.462" \
  "v_edge.1155" vertices "vertex.508" "vertex.504" "vertex.352" \
  "v_vertex.832" reverse periodic
/ For faces where boundary layers will impact, need to link periodic
/ Link top and bottom fluid
face link "bottom" "top" edges "edge.273" "edge.577" "edge.629" "edge.277" \
  "edge.522" "edge.399" vertices "vertex.221" "vertex.425" "vertex.466" \
  "vertex.224" "vertex.387" "vertex.305" reverse periodic
/ BL INWARDS
blayer create "bl-part02-in" first 0.003 growth 1.2 total 0.016104 rows 4 \
  transition 1 trows 0 continuous uniform
blayer attach "bl-part02-in" volume "part2" "part2" "part2" "part2" "part2" \
  "part2" face "part02-hole3" "part02-hole1" "part02-hole2" "part02-1" \
  "part02-3" "part02-2" add
/ BL OUTWARDS
blayer create "bl-part02-out" first 0.001 growth 1 total 0.003 rows 3 \
  transition 1 trows 0 continuous uniform
blayer attach "bl-part02-out" volume "v_cylinder" "v_cylinder" "v_cylinder" \
  "v_cylinder" "v_cylinder" "v_cylinder" face "part02-hole3" "part02-hole1" \
  "part02-hole2" "part02-1" "part02-3" "part02-2" add
blayer create "bl-part01-out" first 0.001 growth 1 total 0.002 rows 2 \
  transition 1 trows 0 continuous uniform
blayer attach "bl-part01-out" volume "v_cylinder" "v_cylinder" "v_cylinder" \
  "v_cylinder" "v_cylinder" "v_cylinder" face "part01-hole3" "part01-hole1" \
  "part01-hole2" "part01-1" "part01-2" "part01-3" add
blayer create "bl-part03-out" first 0.001 growth 1 total 0.002 rows 2 \
  transition 1 trows 0 continuous uniform
blayer attach "bl-part03-out" volume "v_cylinder" "v_cylinder" "v_cylinder" \
  "v_cylinder" "v_cylinder" face "part03-hole3" "part03-hole1" "part03-hole2" \
  "part03-1" "part03-2" add
blayer create "bl-part04-out" first 0.001 growth 1 total 0.002 rows 2 \
  transition 1 trows 0 continuous uniform
blayer attach "bl-part04-out" volume "v_cylinder" "v_cylinder" "v_cylinder" \
```

```
  "v_cylinder" "v_cylinder" face "part04-hole3" "part04-hole1" "part04-hole2" \
  "part04-1" "part04-2" add
blayer create "bl-part05-out" first 0.001 growth 1 total 0.002 rows 2 \
  transition 1 trows 0 continuous uniform
blayer attach "bl-part05-out" volume "v_cylinder" "v_cylinder" "v_cylinder" \
  "v_cylinder" "v_cylinder" face "part05-hole3" "part05-hole1" "part05-hole2" \
  "part05-1" "part05-2" add
blayer create "bl-part06-out" first 0.001 growth 1 total 0.001 rows 1 \
  transition 1 trows 0 continuous uniform
blayer attach "bl-part06-out" volume "v_cylinder" "v_cylinder" "v_cylinder" \
  "v_cylinder" face "part06-hole2" "part06-1" "part06-2" "part06-hole1" add
blayer create "bl-part07-out" first 0.001 growth 1 total 0.001 rows 1 \
  transition 1 trows 0 continuous uniform
blayer attach "bl-part07-out" volume "v_cylinder" "v_cylinder" "v_cylinder" \
  "v_cylinder" face "part07-hole2" "part07-1" "part07-2" "part07-hole1" add
blayer create "bl-part08-out" first 0.001 growth 1 total 0.001 rows 1 \
  transition 1 trows 0 continuous uniform
blayer attach "bl-part08-out" volume "v_cylinder" "v_cylinder" "v_cylinder" \
  "v_cylinder" "v_cylinder" "v_cylinder" face "part08-hole1" "part08-hole2" \
  "part08-1" "part08-3" "part08-2" "part08-hole3" add
blayer create "bl-part09-out" first 0.001 growth 1 total 0.003 rows 3 \
  transition 1 trows 0 continuous uniform
blayer attach "bl-part09-out" volume "v_cylinder" "v_cylinder" "v_cylinder" \
  "v_cylinder" "v_cylinder" face "part09-hole3" "part09-hole1" "part09-1" \
  "part09-2" "part09-hole2" add
blayer create "bl-part12-out" first 0.001 growth 1 total 0.002 rows 2 \
  transition 1 trows 0 continuous uniform
blayer attach "bl-part12-out" volume "v_cylinder" "v_cylinder" "v_cylinder" \
  "v_cylinder" face "part12-hole1" "part12-1" "part12-3" "part12-2" add
/ BL WALL
blayer create "bl-wall" first 0.001 growth 1.2 total 0.0022 rows 2 \
  transition 1 trows 0 continuous uniform
blayer attach "bl-wall" volume "v_cylinder" face "cylinder-wall" add
/ Premesh Troublesome Faces & Edges
edge modify "edge.71" backward
edge mesh "edge.71" "edge.331" successive ratio1 0.97 size 0.037
edge mesh "edge.330" successive ratio1 0.97 ratio2 0.97 size 0.037
edge mesh "edge.769" "edge.770" successive ratio1 0.97 ratio2 0.97 size 0.03
face mesh "part02-hole3" "part02-hole1" "part02-hole2" "part08-hole1" \
  "part08-hole2" triangle size 0.03
/ Mesh all volumes, uniform
volume mesh "part2" "v_part8" "v_part11" "part4" "part5" "part6" "part7" "part3" \
  "part9" "part10" "part1" "part12" "fluid-part11-hole2" \
  "fluid-part11-hole3" "v_cylinder" tetrahedral size 0.03
/
/ END OF MESHING SECTION, START OF ZONES
/
physics create "fluid" ctype "FLUID" volume "fluid-part11-hole2" \
  "fluid-part11-hole3" "v_cylinder"
physics create "part01" ctype "SOLID" volume "part1"
physics create "part12" ctype "SOLID" volume "part12"
physics create "part03" ctype "SOLID" volume "part3"
physics create "part02" ctype "SOLID" volume "part2"
physics create "part04" ctype "SOLID" volume "part4"
physics create "part05" ctype "SOLID" volume "part5"
physics create "part06" ctype "SOLID" volume "part6"
physics create "part07" ctype "SOLID" volume "part7"
physics create "part08" ctype "SOLID" volume "v_part8"
physics create "part09" ctype "SOLID" volume "part9"
physics create "part10" ctype "SOLID" volume "part10"
physics create "part11" ctype "SOLID" volume "v_part11"
window modify 1 AND 2 AND 3 AND 4 invisible mesh
physics create "bottom" btype "WALL" face "bottom" "bottom-part01-hole3" \
```

```
  "bottom-part01-hole2" "bottom-part01-hole1" "bottom-part04-hole3" \
  "bottom-part04-hole2" "bottom-part04-hole1" "bottom-part10-hole3" \
  "bottom-part10-hole2" "bottom-part10-hole1"
physics create "top" btype "WALL" face "top" "top-part05-hole1" \
  "top-part05-hole2" "top-part05-hole3" "top-part11-hole3" "top-part11-hole1" \
  "top-part11-hole2" "top-part03-hole1" "top-part03-hole2" "top-part03-hole3"
physics create "cylinder-wall" btype "WALL" face "cylinder-wall"
physics create "sym1" btype "SYMMETRY" face "sym1" "sym1-part09-hole1" \
  "sym1-part12-hole1" "sym1-part11-hole2" "sym1-part09-hole3" \
  "sym1-part10-hole3"
physics create "sym2" btype "SYMMETRY" face "sym2" "sym2-part07-hole2" \
  "sym2-part07-hole1" "sym2-part06-hole2" "sym2-part06-hole1" \
  "sym2-part10-hole3" "sym2-part11-hole3"
physics create "p1" btype "WALL" face "part01-1" "part01-hole1" \
  "part01-hole2" "part01-hole3" "part01-2" "part01-3"
physics create "p1-b" btype "WALL" face "part01-bottom"
physics create "p2" btype "WALL" face "part02-1" "part02-2" "part02-3" \
  "part02-hole3" "part02-hole1" "part02-hole2"
physics create "p3" btype "WALL" face "part03-1" "part03-2" "part03-hole3" \
  "part03-hole2" "part03-hole1"
physics create "p3-t" btype "WALL" face "part03-top"
physics create "p4" btype "WALL" face "part04-1" "part04-2" "part04-hole1" \
  "part04-hole2" "part04-hole3"
physics create "p4-b" btype "WALL" face "part04-bottom"
physics create "p5" btype "WALL" face "part05-2" "part05-1" "part05-hole3" \
  "part05-hole2" "part05-hole1"
physics create "p5-t" btype "WALL" face "part05-top"
physics create "p6" btype "WALL" face "part06-2" "part06-1" "part06-hole2" \
  "part06-hole1"
physics create "p6-b" btype "WALL" face "part06-bottom-1" "part06-bottom-2"
physics create "p6-s2" btype "WALL" face "part06-sym2"
physics create "p7" btype "WALL" face "part07-2" "part07-1" "part07-hole2" \
  "part07-hole1"
physics create "p7-s2" btype "WALL" face "part07-sym2"
physics create "p7-t" btype "WALL" face "part07-top-1" "part07-top-2"
physics create "p8" btype "WALL" face "part08-2" "part08-1" "part08-3" \
  "part08-hole1" "part08-hole2" "part08-hole3"
physics create "p8-s2" btype "WALL" face "part08-sym2"
physics create "p9" btype "WALL" face "part09-2" "part09-1" "part09-hole1" \
  "part09-hole3" "part09-hole2"
physics create "p9-s1" btype "WALL" face "part09-sym1"
physics create "p10" btype "WALL" face "part10-2" "part10-1" "part10-hole1" \
  "part10-hole2" "part10-hole3"
physics create "p10-b" btype "WALL" face "part10-bottom"
physics create "p10-s1" btype "WALL" face "part10-sym1-1" "part10-sym1-2"
physics create "p10-s2" btype "WALL" face "part10-sym2-1" "part10-sym2-2"
physics create "p11" btype "WALL" face "part11-1" "part11-2" "part11-hole2" \
  "part11-hole3" "part11-hole1"
physics create "p11-t" btype "WALL" face "part11-top"
physics create "p11-s1" btype "WALL" face "part11-sym1"
physics create "p11-s2" btype "WALL" face "part11-sym2"
physics create "p12" btype "WALL" face "part12-2" "part12-1" "part12-3" \
  "part12-hole1"
physics create "p12-s1" btype "WALL" face "part12-sym1"
physics create "p12-s2" btype "WALL" face "part12-sym2-1" "part12-sym2-2"
save
/Write out the mesh
export fluent5 "3-HOLE-WITH-BL.msh"
```

APPENDIX C: BOUNDARY LAYERS

C.1: 3-HOLE

Particle	First layer thickness (inches)	Growth	Number of layers	Total depth (inches)
Wall Boundary Layer				
N/A	0.001	1.2	2	0.0022
Inner Boundary Layers (into the particle)				
2	0.003	1.2	4	0.016104
Outer Boundary Layers (into the fluid)				
1	0.001	1	3	0.003
2	0.001	1	3	0.003
3	0.001	1	2	0.002
4	0.001	1	2	0.002
5	0.001	1	2	0.002
6	0.001	1	1	0.001
7	0.001	1	1	0.001
8	0.001	1	1	0.001
9	0.001	1	3	0.003
12	0.001	1	2	0.002

C.2: 4-HOLE WITH GROOVES

Particle	First layer thickness (inches)	Growth	Number of layers	Total depth (inches)
Wall Boundary Layer				
N/A	0.001	1	2	0.002
Inner Boundary Layers (into the particle)				
2	0.005	1	4	0.02
Outer Boundary Layers (into the fluid)				
1	0.001	1	2	0.002
2	0.001	1	3	0.003
3	0.001	1	2	0.002
4	0.001	1	2	0.002
5	0.001	1	2	0.002
6	0.001	1	1	0.001
7	0.001	1	1	0.001
8	0.001	1	1	0.001
9	0.001	1	1	0.001
12	0.001	1	2	0.002

C.3: 6-HOLE

Particle	First layer thickness (inches)	Growth	Number of layers	Total depth (inches)
Wall Boundary Layer				
N/A	0.001	1.2	2	0.0022
Inner Boundary Layers (into the particle)				
2	0.003	1.2	4	0.016104
Outer Boundary Layers (into the fluid)				
1	0.001	1	2	0.002
2	0.001	1	3	0.003
3	0.001	1	2	0.002
4	0.001	1	2	0.002
5	0.001	1	2	0.002
6	0.001	1	1	0.001
7	0.001	1	1	0.001
8	0.001	1	1	0.001
9	0.001	1	3	0.003
12	--	--	--	--

APPENDIX D: MASS FRACTION BOOTSTRAPPING AND REACTION RATE CONVERGENCE CHECKS

D.1: 3-HOLE MASS FRACTION BOOTSTRAPPING

Bootstrap	User-Defined Scalar	Mass Fraction Value	Difference
0	UDS_0	0.1964685000	
	UDS_1	0.0005314771	
	UDS_2	0.0007304772	
	UDS_3	0.1760670000	
1	UDS_0	0.1963390000	-0.0001295
	UDS_1	0.0005629062	3.14291E-05
	UDS_2	0.0007605496	3.00724E-05
	UDS_3	0.1768239000	0.0007569
2	UDS_0	0.1962114000	-0.0001276
	UDS_1	0.0005942282	0.000031322
	UDS_2	0.0007902082	2.96586E-05
	UDS_3	0.1775704000	0.0007465
3	UDS_0	0.1960858000	-0.0001256
	UDS_1	0.0006253839	3.11557E-05
	UDS_2	0.0008194126	2.92044E-05
	UDS_3	0.1783058000	0.0007354
	UDS_3	0.1964685000	

D.2: 3-HOLE REACTION RATE CONVERGENCE CHECK

Iteration	Reaction/Component	Reaction Rate (kmol/s)	Difference	%Difference
4333	Rxn1	1.9113E-08		
	Rxn2	-5.2085E-09		
	Rxn3	3.1846E-07		
	CH4 Con	-3.3757E-07		
	H2 Prod	1.3260E-06		
	CO Prod	2.4321E-08		
	CO2 Prod	3.1325E-07		
10328	Rxn1	1.9110E-08	2.8000E-12	1.4652E-02
	Rxn2	-5.2039E-09	-4.5800E-12	8.8010E-02
	Rxn3	3.1842E-07	3.6000E-11	1.1306E-02
	CH4 Con	-3.3754E-07	-3.6000E-11	1.0666E-02
	H2 Prod	1.3258E-06	1.6000E-10	1.2068E-02
	CO Prod	2.4314E-08	7.2000E-12	2.9613E-02
	CO2 Prod	3.1321E-07	3.6000E-11	1.1494E-02
14000	Rxn1	1.9112E-08	-1.6000E-12	-8.3718E-03
	Rxn2	-5.2062E-09	2.2500E-12	-4.3218E-02
	Rxn3	3.1844E-07	-1.7000E-11	-5.3386E-03
	CH4 Con	-3.3755E-07	1.8000E-11	-5.3325E-03
	H2 Prod	1.3259E-06	-8.0000E-11	-6.0337E-03
	CO Prod	2.4316E-08	-2.0000E-12	-8.2250E-03
	CO2 Prod	3.1323E-07	-1.6000E-11	-5.1081E-03
17500	Rxn1	1.9119E-08	-6.8000E-12	-3.5568E-02
	Rxn2	-5.2083E-09	2.0800E-12	-3.9936E-02
	Rxn3	3.1849E-07	-5.4000E-11	-1.6955E-02
	CH4 Con	-3.3761E-07	6.0000E-11	-1.7772E-02
	H2 Prod	1.3261E-06	-2.4000E-10	-1.8098E-02
	CO Prod	2.4325E-08	-9.4000E-12	-3.8643E-02
	CO2 Prod	3.1328E-07	-5.2000E-11	-1.6599E-02
24700	Rxn1	1.9123E-08	-4.0000E-12	-2.0918E-02
	Rxn2	-5.2063E-09	-1.9800E-12	3.8031E-02
	Rxn3	3.1851E-07	-1.9000E-11	-5.9653E-03
	CH4 Con	-3.3764E-07	2.4000E-11	-7.1082E-03
	H2 Prod	1.3262E-06	-8.0000E-11	-6.0322E-03
	CO Prod	2.4328E-08	-2.9000E-12	-1.1920E-02
	CO2 Prod	3.1330E-07	-2.0000E-11	-6.3837E-03

D.3: 4-HOLE WITH GROOVES MASS FRACTION BOOTSTRAPPING

Bootstrap	User-Defined Scalar	Mass Fraction Value	Difference
0	UDS_0	0.1965008000	
	UDS_1	0.0005241501	
	UDS_2	0.0007231793	
	UDS_3	0.1758838000	
1	UDS_0	0.1964025000	-9.83E-05
	UDS_1	0.0005484677	2.43176E-05
	UDS_2	0.0007461468	2.29675E-05
	UDS_3	0.1764638000	0.00058
2	UDS_0	0.1963049000	-9.76E-05
	UDS_1	0.0005729199	2.44522E-05
	UDS_2	0.0007689169	2.27701E-05
	UDS_3	0.1770402000	0.0005764
3	UDS_0	0.1962080000	-9.69E-05
	UDS_1	0.0005974638	2.45439E-05
	UDS_2	0.0007914808	2.25639E-05
	UDS_3	0.1776127000	0.0005725
	UDS_3	0.1764638000	0.00058

D.4: 4-HOLE WITH GROOVES REACTION RATE CONVERGENCE CHECK

Iteration	Reaction/Component	Reaction Rate (kmol/s)	Difference	%Difference
3100	Rxn1	2.1825E-08		
	Rxn2	-6.0597E-09		
	Rxn3	3.6427E-07		
	CH4 Con	-3.8610E-07		
	H2 Prod	1.5165E-06		
	CO Prod	2.7884E-08		
	CO2 Prod	3.5821E-07		
6700	Rxn1	2.1822E-08	2.6000E-12	1.1915E-02
	Rxn2	-6.0612E-09	1.4800E-12	-2.4418E-02
	Rxn3	3.6423E-07	3.7000E-11	1.0158E-02
	CH4 Con	-3.8606E-07	-4.1000E-11	1.0620E-02
	H2 Prod	1.5163E-06	2.0000E-10	1.3190E-02
	CO Prod	2.7883E-08	1.1000E-12	3.9450E-03
	CO2 Prod	3.5817E-07	4.2000E-11	1.1726E-02
9700	Rxn1	2.1822E-08	2.0000E-13	9.1651E-04
	Rxn2	-6.0554E-09	-5.8000E-12	9.5782E-02
	Rxn3	3.6425E-07	-1.4000E-11	-3.8435E-03
	CH4 Con	-3.8607E-07	1.0000E-11	-2.5902E-03
	H2 Prod	1.5164E-06	-1.2000E-10	-7.9134E-03

	CO Prod	2.7877E-08	6.3000E-12	2.2599E-02
	CO2 Prod	3.5819E-07	-2.1000E-11	-5.8628E-03
12700	Rxn1	2.1829E-08	-6.7000E-12	-3.0694E-02
	Rxn2	-6.0624E-09	7.0400E-12	-1.1613E-01
	Rxn3	3.6431E-07	-6.7000E-11	-1.8391E-02
	CH4 Con	-3.8614E-07	7.4000E-11	-1.9164E-02
	H2 Prod	1.5167E-06	-2.6000E-10	-1.7143E-02
	CO Prod	2.7891E-08	-1.3900E-11	-4.9837E-02
	CO2 Prod	3.5825E-07	-6.0000E-11	-1.6748E-02
15700	Rxn1	2.1829E-08	-5.0000E-13	-2.2905E-03
	Rxn2	-6.0706E-09	8.1800E-12	-1.3475E-01
	Rxn3	3.6423E-07	8.4000E-11	2.3062E-02
	CH4 Con	-3.8615E-07	6.0000E-12	-1.5538E-03
	H2 Prod	1.5167E-06	-2.0000E-11	-1.3187E-03
	CO Prod	2.7900E-08	-9.4000E-12	-3.3691E-02
	CO2 Prod	3.5825E-07	0.0000E+00	0.0000E+00
18700	Rxn1	2.1827E-08	1.9000E-12	8.7048E-03
	Rxn2	-6.0709E-09	3.1000E-13	-5.1063E-03
	Rxn3	3.6428E-07	-5.4000E-11	-1.4824E-02
	CH4 Con	-3.8611E-07	-3.8000E-11	9.8417E-03
	H2 Prod	1.5166E-06	1.3000E-10	8.5720E-03
	CO Prod	2.7898E-08	2.5000E-12	8.9613E-03
	CO2 Prod	3.5821E-07	3.7000E-11	1.0329E-02
24700	Rxn1	2.1824E-08	3.6000E-12	1.6496E-02
	Rxn2	-6.0553E-09	-1.5660E-11	2.5862E-01
	Rxn3	3.6427E-07	1.9000E-11	5.2160E-03
	CH4 Con	-3.8609E-07	-1.8000E-11	4.6621E-03
	H2 Prod	1.5165E-06	7.0000E-11	4.6159E-03
	CO Prod	2.7879E-08	1.9100E-11	6.8511E-02
	CO2 Prod	3.5821E-07	2.0000E-12	5.5833E-04

D.5: 6-HOLE MASS FRACTION BOOTSTRAPPING

Bootstrap	User-Defined Scalar	Mass Fraction Value	Difference
0	UDS_0	0.1964685000	
	UDS_1	0.0005314771	
	UDS_2	0.0007304772	
	UDS_3	0.1760670000	
1	UDS_0	0.1963390000	-0.0001295
	UDS_1	0.0005629062	3.14291E-05
	UDS_2	0.0007605496	3.00724E-05
	UDS_3	0.1768239000	0.0007569
2	UDS_0	0.1962114000	-0.0001276
	UDS_1	0.0005942282	0.000031322
	UDS_2	0.0007902082	2.96586E-05
	UDS_3	0.1775704000	0.0007465
3	UDS_0	0.1960858000	-0.0001256
	UDS_1	0.0006253839	3.11557E-05
	UDS_2	0.0008194126	2.92044E-05
	UDS_3	0.1783058000	0.0007354
	UDS_3	0.1964685000	

D.6: 6-HOLE REACTION RATE CONVERGENCE CHECK

Iteration	Reaction/Component	Reaction Rate (kmol/s)	Difference	%Difference
5874	Rxn1	2.2240E-08		
	Rxn2	-6.0507E-09		
	Rxn3	3.6910E-07		
	CH4 Con	-3.9134E-07		
	H2 Prod	1.5371E-06		
	CO Prod	2.8290E-08		
	CO2 Prod	3.6304E-07		
10008	Rxn1	2.2237E-08	2.3000E-12	1.0343E-02
	Rxn2	-6.1039E-09	5.3270E-11	-8.7272E-01
	Rxn3	3.6907E-07	3.7000E-11	1.0025E-02
	CH4 Con	-3.9130E-07	-4.0000E-11	1.0222E-02
	H2 Prod	1.5369E-06	2.0000E-10	1.3013E-02
	CO Prod	2.8340E-08	-5.0600E-11	-1.7854E-01
	CO2 Prod	3.6295E-07	9.4000E-11	2.5899E-02
13413	Rxn1	2.2266E-08	-2.8100E-11	-1.2620E-01
	Rxn2	-6.1162E-09	1.2260E-11	-2.0045E-01
	Rxn3	3.6922E-07	-1.5700E-10	-4.2522E-02
	CH4 Con	-3.9149E-07	1.8700E-10	-4.7767E-02
	H2 Prod	1.5376E-06	-6.9000E-10	-4.4876E-02
	CO Prod	2.8381E-08	-4.0500E-11	-1.4270E-01
	CO2 Prod	3.6309E-07	-1.4300E-10	-3.9384E-02
19918	Rxn1	2.2244E-08	2.1100E-11	9.4855E-02
	Rxn2	-6.1105E-09	-5.6900E-12	9.3119E-02
	Rxn3	3.6911E-07	1.1900E-10	3.2240E-02
	CH4 Con	-3.9135E-07	-1.4100E-10	3.6030E-02
	H2 Prod	1.5370E-06	5.2000E-10	3.3831E-02
	CO Prod	2.8354E-08	2.6800E-11	9.4519E-02
	CO2 Prod	3.6298E-07	1.1100E-10	3.0580E-02